Original Research Article

Surface-Decorated Nanocarrier as a Targeted Drug Delivery Cargo to Folate Receptor-Overexpressing Cells for Auspicious Anti-cancer and Anti-inflammatory Activity

ABSTRACT

Aims: Folate receptor (FR) is overexpressed in most cancer cells and activated macrophages entailed in rheumatoid arthritis (RA). The aim of the current study is the fabrication of FR-targeted nanocarrier loaded with methotrexate (MTX) to magnify its therapeutic efficacy and limit its toxicity.

Methodology: Folic acid-chitosan (FA-CS) conjugate was synthesized and characterized. MTX loaded poly(d,l-lactide-co-glycolide) (PLGA) nanoparticles (NPs) were prepared, optimized and coated with different concentrations of FA-CS conjugate. The selected FA-CS coated MTX NPs formulation (F10) was evaluated via *in vitro* and *in vivo* studies.

Results: F10 had satisfactory encapsulation efficiency (76.2%), homogenous particle size (278.6 nm) and positive zeta potential (34.0 mV) and displayed biphasic drug release pattern in different pH media. Further characterization of F10 cinched MTX incorporation in the polymeric matrix of the targeted nanocarrier. *In vitro* cytotoxicity assay to FR-positive and FR-negative cancer cells revealed the improved anticancer effect of F10 to FR-positive cancer cells, which was absent in FR-negative cells, compared to free MTX or uncoated MTX NPs (F2). F10 showed appropriate storage stability at refrigerated temperature up to 3 months. Moreover, oral administration of F10 in treatment of complete Freund's adjuvant (CFA)-induced RA in BALB/c mice conferred prodigious therapeutic outcomes and declined systemic toxicity compared to oral treatment with conventional pure MTX or commercial MTX tablets.

Conclusion: The fabricated targeted nanocarrier could enhance anticancer activity of MTX to FR-overexpressing cancer cells and could be a promising novel approach for oral administration of MTX in treatment of RA or other inflammatory conditions associated with FR-overexpressing activated macrophages.

Keywords: *methotrexate; folic acid-chitosan conjugate; PLGA nanoparticles; oral drug delivery; complete Freund's adjuvant-induced arthritis.*

1. INTRODUCTION

One of the unresolved limitations of conventional therapies is their non-specific distribution to off-target sites, resulting in marked toxicity and declined curative efficiency due to limited available dose at the target sites [1]. Nanoparticulate drug delivery systems can be furnished with particular ligand molecules such as folic acid (FA), mannose, galactose, transferrin, and antibodies that can precisely deliver nanocarriers to receptors that are preferentially expressed on specific cells for targeted drug delivery [2].

Folate receptor (FR) is overexpressed in most cancers, including breast and cervical cancers [1, 3], besides activated macrophages that play a critical role in development of inflammatory and autoimmune diseases such as rheumatoid arthritis (RA) [4] and psoriasis [5, 6]. FA is extensively utilized in active targeting of attached nanocarriers to cancers and activated macrophages [4] because of the convenience of its conjugation, its high binding affinity to FR [5], besides being inexpensive, neither toxic nor immunogenic, and stable upon storage and application [2, 7, 8].

Polymeric nanoparticles (NPs) are versatile nanocarriers that can prominently improve drug delivery by various merits as targeted delivery, enhanced bioavailability, protection against enzymatic degradation, and controlled release [9]. Poly(d,l-lactide-co-glycolide) (PLGA) is FDA approved polymer for use in therapeutic and clinical applications[9, 10]. Unsatisfactorily, PLGA NPs suffer from burst drug release, limited drug retention in targeted tissue [9], limited application in oral delivery [11], and rapid clearance from the blood by opsonization [12], owing to their negative surface charge [11]. Surface modification of PLGA NPs with FA can be achieved through coating with chitosan (CS). CS coating of PLGA NPs can improve cellular interactions of NPs [13], solve burst drug release associated with PLGA NPs [14], enable targeting ligand functionalization on the surface of PLGA NPs through its conjugation to CS free amino groups [15], and improve bioavailability and efficacy of loaded drugs. Therefore, surface functionalization with FA and CS

*

serves two functions; FA maintains targeting potential, while CS improves PLGA NPs limitations. FA-CS coated PLGA NPs have been recently investigated in drug targeting to FR-overexpressing cancer cells and have boosted the anticancer activity of their drug payloads, particularly bicalutamide [8] and docetaxel [9] to FR-overexpressing cancer cells. However, oral administration of FA-CS coated PLGA NPs as targeted drug delivery system has never been evaluated *in vivo* yet.

Methotrexate (MTX) is a chemotherapeutic agent used in the treatment of tumors such as leukemia, breast and lung cancers as well as in the management of inflammatory and autoimmune conditions such as RA, psoriasis, and multiple sclerosis [16]. MTX is the drug of choice in treatment of early RA [17]. However, MTX use is limited due to its low bioavailability and its short half-life due to its rapid renal elimination [16]. Moreover, its long term adherence and tolerance is fraught by its off-targeted delivery and multiple systemic toxicities, significantly influencing the overall wellness of patients [16-19]. Recently, various MTX targeted nanocarriers have been investigated in cancer therapy as polymeric NPs [20, 21], hybrid polymer NPs [22], and in RA treatment like yeast glucan [18] and dextran-based NPs [19], and hydroxyapatite NPs [23], aiming to improve its bioavailability, efficacy and reduce its undesirable effects. However, neither of MTX targeted nanosystems has studied their therapeutic effects upon oral administration in treatment of complete Freund's adjuvant (CFA)-induced RA model in mice. Thus, development of a novel oral MTX targeted nanocarrier in treatment of RA is still required and can be of great interest as oral drug delivery is the most prevalent and most preferred approach of drug administration due to its higher convenience, efficacy, higher patient compliance, and non-invasiveness [24].

To the best of our knowledge, no attempts have inspected the preparation of FA-CS coated PLGA NPs loaded with MTX to target its delivery to FR-overexpressing cells, either cancers or activated macrophages. Therefore, the aim of the current investigation was to prepare FA decorated MTX nanocarrier to actively target its delivery to FR-overexpressing cells. *In vitro* cytotoxicity assay was performed to evaluate the anticancer efficacy of the developed targeted MTX nanocarrier to FR-positive and FR-negative cancer cells. Additionally, the prepared targeted MTX nanocarrier delivery to FR-overexpressing activated macrophages upon oral administration was assessed via *in vivo* therapeutic efficacy and toxicity study in treatment of CFA-induced RA mice model and compared to oral administration of pure MTX and commercial MTX tablets preparation.

2. MATERIAL AND METHODS

2.1 Materials

MTX and FA were obtained as a gift from EIMC United Pharmaceuticals (Badr City, Egypt) and NAPCO Pharm (10th of Ramadan City, Egypt), respectively. PLGA [lactide: glycolide ratio 50:50; PURASORB® PDLG 5002A (carboxylic acid terminated copolymer, viscosity = 0.16 – 0.24 dL/g)] was kindly gifted by Corbion Purac Biomaterials (Gorinchem, Netherlands). CS (low molecular weight of 50 - 190 kDa; 75 - 85% deacetylated), dialysis tubing cellulose membrane (molecular weight cut off = 12 - 14 kDa), dialysis tube closures, and CFA (1 mg heat-killed Mycobacterium tuberculosis/mL paraffin oil) were purchased from Sigma Aldrich (Saint Louis, MO, USA). Polyvinyl alcohol (PVA) (molecular weight of 31 - 50 kDa) and 1-ethyl-3-(3-dimethylaminopropyl) carbodiimide hydrochloride (EDC) were purchased from Acros organics (Geel, Antwerp, Belgium). Dimethyl sulfoxide (DMSO) and glacial acetic acid were purchased from Fisher Scientific (Leicestershire, UK). Dichloromethane (DCM) was procured from Adwic, EL Nasr Pharmaceutical Chemicals Co. (Cairo, Egypt). All other chemicals were of fine analytical grade. Cell lines, namely; human breast cancer cells (MCF-7), human cervical cancer cells (HeLa), and human lung cancer cells (A549), were obtained from American Type Culture Collection (Manassas, VA, USA) through holding company for biological products and vaccines VACSERA (Cairo, Egypt). RPMI-1640 medium, Fetal Bovine Serum (FBS), and 3-(4, 5-dimethylthiazol-2-yl)-2,5-diphenyltetrazolium bromide (MTT) were purchased from Lonza (Allendale, USA). Rheumatoid factor (RF) latex kits were obtained from Atlas Medical (Berlin, Germany). Tumor necrosis factor-alpha (TNF-α) enzyme-linked immunosorbent assay (ELISA) kit (number: SEA133Mu) and interleukin-1 beta (IL-1β) ELISA kit (number:SEA563Mu) were obtained from Cloud-Clone Corp. (Texas, USA). Interleukin-k (IL-6) ELISA kit (cataloug #: ADI-900-045) was obtained from ENZO Life Sciences (Barcelona, Spain). Serum aspartate transaminase (AST), alanine transaminase (ALT) kits were purchased from Agappe Diagnostics Ltd., (Kerala, India). Serum creatinine (CR) and blood urea nitrogen (BUN) kits were purchased from Diamond Diagnostics (Holliston MA, USA).

2.2 Synthesis of FA-CS Conjugate

FA and CS conjugation approached by two main steps as previously reported [2]. Firstly, FA (0.73 g) and EDC (0.69 g) were dissolved in anhydrous DMSO and magnetically stirred (MS300HS, MTOPS Corp., Korea) for 1h in the dark at room temperature to activate FA terminal carboxylic acid group (COOH). CS (0.59 g) was dissolved in 300 mL acetate buffer solution (pH 4.7). Then, the activated FA solution was slowly added to CS solution. The reaction was allowed to proceed by stirring for 16 h at room temperature. FA-CS was precipitated by adding 1M NaOH till pH 9 and was further purified by dialysis against PBS (pH 7.4) for 3 days and then against deionized water (DW) for another 3 days. Finally, the yellowish-orange conjugate was gained by filtration and lyophilization at -80°C for 48h (Freeze dryer, SIM FD8-8 T, SIM international, USA).

Afterwards, the prepared FA-CS conjugate was thoroughly characterized. Fourier transform infra-red (FTIR) spectra of FA, CS and FA-CS conjugate were recorded on an FTIR spectrometer (Madison Instruments, Middleton, WI, USA) in the range 400 - 4000 cm^{-1}, utilizing the KBr pellet technique. Proton nuclear magnetic resonance (^{1}H NMR) spectra were recorded on (Bruker Avance III HD FT-high resolution (400 MHz), Fällanden, Switzerland) spectrophotometer, using deuterated DMSO as solvent for FA and deuterated water containing 1% deuterated trifluoroacetic acid for CS and FA-CS [7, 25]. Differential scanning calorimetry (DSC) thermograms and X□ray diffraction (XRD) patterns of FA, CS, and FA-CS conjugate were recorded using differential scanning calorimeter (Shimadzu DSC 50, Tokyo, Japan) and X-ray diffractometer (Rigaku Rint-2500VL, Tokyo, Japan), respectively.

2.3 Preparation of MTX Loaded PLGA NPs

Uncoated NPs were prepared by modified double emulsion method (W/O/W) adopted from previously reported methodology with some modifications [16, 26]. Drug polymer weight ratio was maintained at 1:5 and 1:10, different polymer PLGA weight % were carried out (1%, 2%, and 4% w/v) and varying stabilizer PVA concentrations (1% and 2% w/v) were utilized, as shown in Table 1. Firstly, accurately weighed amount of PLGA was dissolved in 5 mL DCM and corresponding weighed amount of MTX was solubilized in 1 mL DMSO. PLGA and MTX solutions were emulsified with probe ultrasonication (Sonics Vibra-cell™, Model VC 505, Sonic & Materials, Inc., USA) at 100% amplitude for 2 min and 30 sec to form the primary emulsion. Then, 10 mL of PVA solution, as the outer aqueous phase, were added and emulsified in drug/polymer solution by probe ultrasonication at 100% amplitude for 2 min and 30 sec to accomplish the desired double emulsion. Afterwards, 20 mL of either 0.05 or 0.2% (w/v) PVA solution was added to dilute the preparation. Ultrasonication was performed in an ice bath. Finally, the prepared emulsion left on magnetic stirrer overnight at 800 rpm at room temperature to evaporate the organic solvent. NPs were collected by cooling centrifugation at 13000 rpm and 4°C for 2 h (Cooling centrifuge, CE16-4X100RD, ACCULAB, USA). The clear supernatant was carefully collected and the sedimented MTX NPs pellets were washed with DW, resuspended in DW, lyophilized and subsequently stored at 4°C for further characterization. Nine formulations (F1-F9), as shown in Table 1, were prepared to study the effect of polymer, drug, and stabilizer concentrations on the prepared NPs. Corresponding plain NPs were prepared by the same method. The selected uncoated MTX NPs (F2) dispersion was further coated with FA-CS solution in (1%) acetic acid solution prepared at two different concentrations (0.1 and 0.2% w/v) to fabricate two batches of the desired FA-CS coated MTX nanocarrier, F10 and F11, respectively. FA-CS solution was then added dropwise to equivalent volume of F2 dispersion with ratio of suspension 1:1 under magnetic stirring at 800 rpm at room temperature. The mixture was incubated for further 90 min and then NPs were collected by cooling centrifugation at 13000 rpm and 4°C for 2 h. The clear supernatant was carefully collected and the sedimented FA-CS coated MTX NPs pellets were washed with DW, resuspended in DW, and lyophilized. Subsequently, lyophilized formulated FA-CS coated MTX NPs were stored at 4°C for further characterization. Plain FA-CS coated NPs were prepared by the same procedures.

2.4 Characterization of MTX Loaded NPs

2.4.1 Encapsulation Efficiency Percent (EE%)

MTX EE% was directly determined [26]. MTX loaded NPs were dissolved in DMSO with the aid of sonication in a bath sonicator (Sonix IV USA, SS101H230) for 10 min to ensure complete dissolution of all NPs. After appropriate dilution with DMSO, EE% was assayed spectrophotometrically (ultraviolet-visible double beam spectrophotometer; Labomed Inc., USA) at 297 nm against plain NPs that were treated similarly. EE% was calculated according to the following equation [8, 27]:

$$\text{EE\%} = \frac{\text{Amount of MTX entrapped}}{\text{Amount of MTX initally added}} \times 100$$

2.4.2 Particle Size (PS), Polydispersity Index (PDI) and Zeta Potential (ζP) Determination

The average PS, PDI, and ζP of all the freshly prepared samples of MTX loaded NPs were analyzed in triplicate by Zetasizer (Malvern Instruments, Malvern, UK). PS and PDI determination utilized dynamic light scattering (DLS) mechanism, while ζP employed Laser Doppler Anemometry (LDA) technique, which records the electrophoretic mobility of the NPs under an electric field. Samples were appropriately diluted with DW prior to measurements.

2.4.3 *In Vitro* Release and Kinetics Analysis

The dialysis bag diffusion method was equipped to evaluate the in vitro release pattern of MTX from the optimized freshly prepared uncoated formulation (F2) and either 0.1% or 0.2% FA-CS coated formulation F10 and F11, respectively, and to compare their release patterns with that of free MTX as control from each release medium [16, 21, 28]. The experiment was held in three different pH values (1.2, 6.8, and 7.4). Briefly, F2, F10, and F11, containing an equivalent 3 mg MTX, were dispersed in 3 mL of each release medium and then placed in a dialysis membrane that was equilibrated overnight with the respective release medium. Both ends of the bag were sealed with closures and immersed in 100 mL of each release medium and kept in a thermostatically controlled shaking incubator (GFL Gesellschaft für Labortechnik, Burgwedel, Germany) that was kept at 37 ± 0.5 °C with moderate agitation (100 rpm) throughout the whole experiment. At predetermined time intervals of 0.5, 1, 2, 3, 4, 5, 6, 7 and 8 h, an aliquot of 3 mL was collected and equivalent volume of fresh medium was added. Drug concentration was then quantified spectrophotometrically at 303 nm [29]. Plain NPs were treated similarly and used as blank. The release study was conducted in triplicate and percentage of cumulative MTX released was determined. Release data were processed in various kinetic models [30-32] to determine the mechanism of drug release as reported earlier [33].

2.4.4 Fourier Transform Infrared Spectroscopy (FTIR)

The FTIR spectra of pure MTX, PLGA, PVA, FA-CS conjugate, their physical mixture at similar ratio to that of the optimized FA-CS coated MTX NPs formulation (F10), the optimized lyophilized FA-CS coated MTX NPs formulation (F10), and its plain one were obtained in the range of 400 – 4000 cm^{-1} utilizing KBr methodology.

2.4.5 Differential Scanning Calorimerty (DSC)

DSC analysis was employed for pure MTX, PLGA, PVA, FA-CS conjugate, their physical mixture analogues to the optimized FA-CS coated MTX NPs formulation (F10), the lyophilized form of the optimized FA-CS coated MTX NPs formulation (F10), and its plain

one using a differential scanning calorimeter. The DSC runs were calibrated with Indium, a reference standard with purity of 99.99% and melting point of 156.6°C. In a hermetically sealed aluminum pan, few milligrams of each sample were heated over temperature range from to 30°C to 400°C under constant purging of dry nitrogen at 45 mL/min and at heating rate of 10°C/min.

2.4.6 X-Ray Diffractometry (XRD)

XRD patterns of MTX, PLGA, PVA, FA-CS conjugate, their physical mixture alike the optimized FA-CS coated MTX NPs formulation (F10), the lyophilized form of the selected FA-CS coated MTX NPs formulation (F10), and its corrosponding plain formulation were revealed by X-ray diffractometer furnished with Co-Kα radiation. All diffraction examinations were conducted at two theta angle with voltage of 45 kV and a current of 40 mA.

2.4.7 Transmission Electron Microscopy (TEM)

Morphological changes between the optimum uncoated (F2) and the selected FA-CS coated MTX NPs formulation (F10) were visualized by transmission electron microscopy (TEM) (JEOL JEM-2100, JEOL Ltd., Tokyo, Japan) and images were captured by a digital micrograph and analyzed by imaging viewer software. A tiny drop from each formulation dispersion, adequately diluted in DW and sonicated for 5 min, was located on carbon-coated copper grid. Subsequently, excessive material was blotted with filter paper and eventually grid was air dried at room temperature for contrast enhancement, and then inspected via TEM without staining.

2.5 *In Vitro* Cytotoxicity Assay

The cytotoxicity of free MTX, uncoated MTX NPs (F2) and FA-CS coated MTX NPs (F10), together with corrosponding plain NPs of uncoated and FA-CS coated NPs was assesed to evaluate the anticancer activity against FR-positive MCF-7, HeLa, and FR-negative A549 cancer cells and screened via MTT assay [21, 33]. The cells were cultivated in RPMI-1640 growth media supplemented with 10% FBS and seeded in flat-bottom 96-well plates for cell confluency. Subsequently, all tested cells were treated with different concentrations ranging from (0.05 to 500 µg/mL) of the uncoated MTX NPs (F2) and FA-CS coated MTX NPs (F10) and free MTX, along with corrosponding plain NPs that were treated similarly. The plates were incubated in humified atmosphere with 5% CO_2 at 37°C for 24 h. Afterwads, twenty microliter of filtered MTT solution (5 mg/mL in PBS, pH 7.4) was added and mixed with the cells and incubated in the dark for more 4 h at 37°C. The formed formazan crystals were mixed with 200 µL of acidic isopropanol with additional incubation for 1 h. The absorbance was read by microplate reader (Biotek instruments, Inc., Winooski, VT, USA) at 570 nm and percent cell viability was determined by the following equation [21]:

$$\%\ \text{Cell viability} = \frac{\text{absorbance of treated cells}}{\text{absorbance of untreated cells (control)}} \times 100$$

2.6 Storage Stability Study

The freshly prepared optimized FA-CS coated MTX NPs (F10) suspension was packed in screw capped amber glass vials and stored at refrigrated (4 ± 1°C) and ambient conditions (25 ± 2 °C/40 ± 5% relative humidity) [34] for three months to inspect the impact of the storage temperature on physical appearance, PS, PDI, ζP, and EE% that were determined at time zero and then monthly [35].

2.7 *In Vivo* Evaluation of Therapeutic Efficacy and Safety

2.7.1 Animals

All experimental procedures were examined and approved by the Research Ethics Committee, Faculty of Pharmacy, Mansoura University, Egypt (Ethical approval code: 2017 - 60). The experiments were conducted in congruity with the National Institute of Health guidelines of "Principles of Laboratory Animal Care" (NIH publication No. 85 - 23, updated 1985). A total of 36 BALB/c male mice (12 - 14 week-old, 30 - 35 g) obtained from the Medical Experimental Research Center, Mansoura University, Mansoura, Egypt, were employed to scout the therapeutic and anti-inflammatory efficacy, along with the safety of the fabricated targeted MTX nanocarrier in CFA-induced RA in mice compared to pure MTX, and commercial MTX tablets preparation. Animals were housed in the Animal House, Faculty of Pharmacy, Mansoura University, Mansoura, Egypt, one week before the experiment to permit adequate acclimation under standard laboratory conditions of controlled temperature (25 ± 1°C), humidity (55 ± 5%), and lighting with a typical (12 h light/12 h dark cycles) with free access to water and standard laboratory food.

2.7.2 Complete Freund's Adjuvant (CFA)-Induced Arthritis and Treatment Protocol

Mice model of rheumatoid arthritis (RA) was implemented as mentioned earlier [36]. An intraplantar injection of 100 µL of CFA was administered into right hind paw. After one hour, another 100 µL of CFA was subcutaneously injected at the base of the tail. To ensure high incidence of arthritis and potentiate the systemic effects, another booster dose of 100 µL of CFA was subcutaneously administered into the base of the tail on the following day. Mice were monitored every two days for observaion of arthritis. After fourteen days, based on the development of symptoms, treatment was commenced orally via intragastric tube and extended for three weeks. Mice were randomly assigned into six groups (n = 6 per group).

Group 1: Normal control.
Group 2: CFA-induced RA mice (non-treated)
Group 3: Orally treated CFA-induced RA mice by pure MTX.
Group 4: Orally treated CFA-induced RA mice by commercial MTX tablets.
Group 5: Orally treated CFA-induced RA mice by plain FA-CS coated NPs.

Group 6: Orally treated CFA-induced RA mice by FA-CS coated MTX NPs (F10).
Mice received oral treatment with same doses of MTX of 5 mg/kg body weight, on day 14, 17, 20, 23, 26, 29, and 32 post induction [18, 37].

2.7.3 Blood and Tissue Collection and Serum Separation

Twenty four hours after the last treatment, mice were euthanized by thiopental (120 mg/kg/i.p.) [38] and blood samples were obtained from the heart, poured into centrifuge tubes, allowed to stand to coagulate at room temperature, and then centrifuged at 4000 rpm for 10 min (MSE centrifuge, UK) for biochemical quantification. In addition, whole blood samples were collected for estimation of hematological parameters. Right hind paws of experimental animals were instantly excised, washed thoroughly with ice cold saline, and sliced into two parts. One part was stored at -80 □C for further ELISA processing and measurements, while the other paw part was fixed in 10% buffered-formalin for histopathological evaluation. Abdominal cavities of animals were opened; then, livers and kidneys were detached, washed with ice-cold saline and fixed in 10% buffered-formalin for 24 h for histopathological studies.

2.7.4 Assessment of Arthritis Macroscopical Changes and Serum Rheumatoid Factor (RF) Levels

The pathological process of arthritis was evaluated visually by an independent observer, who checked mice weekly in a randomized order and graded the intensity of arthritis according to the modified 5 point scale [36]; 0: no signs of erythema or edema, 1: confined erythema with no edema, 2: mild edema and erythema, 3: moderate to severe erythema and edema, and 4: severe erythema and edema with hardness in movement. Arthritis index of each mouse was expressed as the sum of severity in both hind paws, with maximum of 8 [36]. Fluctuations in paw thickness of all mice in all experimental groups was monitiored by measuring by digital Vernier caliper on everyday of treatment administration [39] in a randomized order, where each group was assessed at a different time at each measuring done. Additionally, on day 33 before euthanasia, photographs and X-ray radiographs of affected paws were recorded (DRTECH, Gyeonggi-do, Republic of Korea) of affected paw. RF was measured in serum by respective commercial latex kit according to the instructions of the manufaturer.

2.7.5 Determination of Pro-inflammatory Cytokines

TNF-α, IL-1β and IL-6 levels in paw homogenate were quantified by ELISA. Briefly, 10% of paw homogenate was prepared in 0.05 M phosphate buffer (pH 7) using a polytron homogenizer at 4□C. The homogenate was centrifuged at 10,000 rpm for 20 min to obtain clear supernatant, from which quanitification was performed using commercially respective ELISA kits following the manufacturers' instructions. Levels of cytokines in paw homogenate were expressed as pico gram per mg protein (pg/mg protein).

2.7.6 Histopathological Analysis

Formalin fixed right hind paw was histologically processed to make a paraffin block, cut into 5 µm sections, and stained by hematoxylin and eosin (H&E) [17]. Stained sections were examined under a light microscope by a professional pathologist in a blinded manner. The severity of the histopatholgical evaluation of the paw tissue was scored as earlier established method [40]. Additionally, formalin-fixed hepatic and renal tissues were washed, dehydrated by a series of increasing alcohol concentrations, and embedded in a paraffin and cut into 5 µm thick stained with H&E and histologically analyzed under a light microscope.

2.7.7 Body Weight Measurements

Changes in body weight were monitored for all experimental animals since the commencement of treatment protocol (day 14) till the end of the study.

2.7.8 Hematological and Biochemical Parameters Determinations

Freshly collected blood samples were subjected to complete blood count (CBC) analysis, including red blood cells (RBC), white blood cells (WBC), and hemoglobin and platelet (PLT) levels, by hematological analyzer (DIAGON Ltd., Budapest, Hungary). Serum AST, ALT, CR, and BUN levels were determined by kinetic calorimetric measurements using respective kits according to the protocol of the manufacturers.

2.8 Statistical Analysis

Statistical analysis using One-way ANOVA followed by Tukey's multiple comparisons tests was performed for all data through GraphPad Prism 8.4.3 software computer program (GraphPad Software, San Diego, CA, USA). Statistical analysis of data was accomplished at $p<0.05$.

3. RESULTS AND DISCUSSION

3.1 Synthesis and Characterization of FA-CS Conjugate

FA was coupled to CS through carbodiimide reaction to attain FA-CS conjugate, Figure 1. The γ-carboxylic group of FA is more reactive so more liable to coupling reaction [25]. Primarily, γ-COOH of FA reacted with EDC, a popular crosslinking agent for coupling of biological compounds presenting carboxylic groups and amines, to form a reactive intermediate that further reacted with amino group of CS to produce a stable conjugate via amide linkage under homogenous conditions [7].

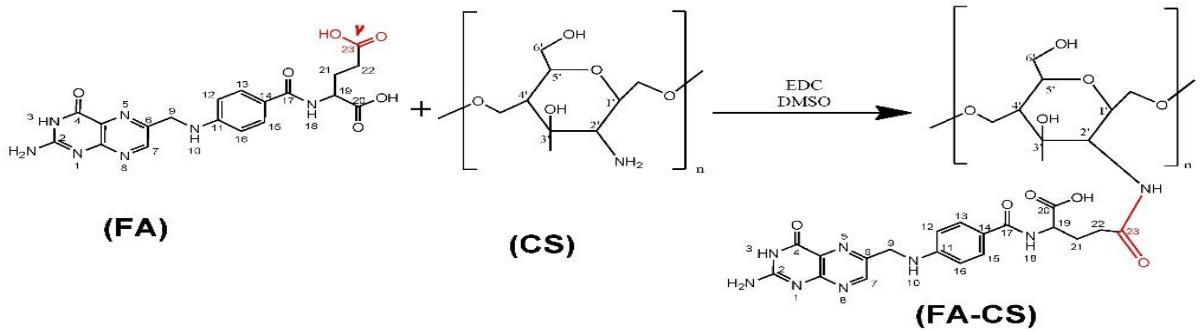

Fig. 1. Graphical representation of FA-CS conjugation reaction.

FTIR spectra of FA, CS and FA-CS conjugate are depicted in Figure 2(A). FA spectrum (I) showed the bands at 3415, 1694, and 1604 cm^{-1} due to N-H stretching vibration, stretching vibration of C=O of carboxylic group, and N-H group bending, respectively [41]. The spectrum of CS (II) exhibited characteristic peaks at 3451, 1656, 1595, 1158, 1074 and 1030 cm^{-1} attributed to overlap between N─H and O─H bands because of intramolecular hydrogen bonds, C=O stretching vibrations of amide I, N-H bending vibrations of amide II, C-O-C bond asymmetric vibration, and C–O stretching vibration, respectively [35]. The spectrum of FA-CS conjugate (III) revealed significant changes compared to that of FA and CS. The disappearance of the peak of the carboxylic group of FA at 1694 cm^{-1} confirmed the formation of amide bond between carboxylates of FA and amino groups of CS [25, 42-44]. Additionally, intensity of absorption peak at 3451 cm^{-1} was augmented and broadened due to overlapping between NH- and OH- stretching vibrations of FA and CS [25]. Moreover, the peak at 1654 cm^{-1} could be referred to -CONH (amide) bond stretching due to interaction FA and CS [42, 43], besides the new peak at 1570 cm^{-1} was related to N-H bending vibration of amide II [25, 45, 46]. These findings aligned with earlier reports, confirming the propitious conjugation between FA and CS via amide bond [42-44].

The structures of FA, CS, and the prepared FA-CS conjugate were revealed by the ^{1}H NMR spectroscopy, Figure 2(B). FA spectrum (I) showed peaks at 8.66, 8.15, 7.65, 6.97, 6.64, 4.49, 4.34, 2.51, and 2.33 ppm related to protons at C7 of pterine ring, at C18, H─C13/C15, H─C10, H─C12/C16, H─C9, H─C19, H─C22, and H─C21, respectively [41, 47]. CS spectrum (II) revealed characteristic peaks at 2.00 and 3.4 - 3.8 ppm assigned to protons of the acetamide group and sugar moiety, respectively [25, 48]. Apparently, spectrum of FA-CS conjugate (III) involved signals derived from both FA and CS. Signals at 8.01, 7.14, and 6.77 ppm were assigned to aromatic protons of FA [2] and signal at 2.42 ppm related to proton of C22 of FA, whereas peak at 1.95 ppm was assigned to CS acetamido group [25, 46]. Successful grafting of FA onto CS was illustrated by the presence of respective peaks in FA-CS spectrum. The findings aligned with earlier results [2, 46, 47].

In Figure 2(C), DSC thermogram of FA (I) depicted three sharp endothermic peaks at 155.88°C, 208.28°C, and 269.11°C, which attributed to breakage of glutamic acid moiety accompanied by loss of pterin and p-aminobenzoic acid moieties[49]. DSC thermogram of CS (II) showed an endothermic peak at 93.4°C and an exothermic one at 305.07°C due to dehydration and polymer degradation, respectively [48]. There was no sharp melting point in the thermogram of FA-CS conjugate (III) with a noticeable shift of the peaks to 79.67°C and 266.01°C, which might be attained to interference of FA coupling to CS crystalline property, confirming FA-CS conjugation [8].

In accordance to Figure 2(D), XRD pattern of FA (I) revealed its crystallinity manifested by several peaks at 2θ of 5.38°, 10.83°, 13.04°, 16.94°, 17.86°, 19.27°, 21.74°, 26.73°, 27.12°, 27.78°, 29.43°, and 31.32° [7, 47]. CS (II) crystallinity was epitomized by strong peaks at 2θ values of 20.03° and 27.83° [47]. Contrarily, diffractogram of FA-CS conjugate (III) displayed a hump peak at 2θ of 20.56° with significant reduction in its intensity probably due to reduction in the crystallinity of FA-CS than that of CS due to strong hydrogen bonds occurred during the conjugation between FA and CS [9, 25], along with the obstructed movement of CS chains due to more complex structure of FA compared to amino group [7, 47]. Collectively, FTIR, ^{1} H NMR, XRD and DSC results of FA-CS conjugate are in concordance with the conclusion of FA and CS coupling.

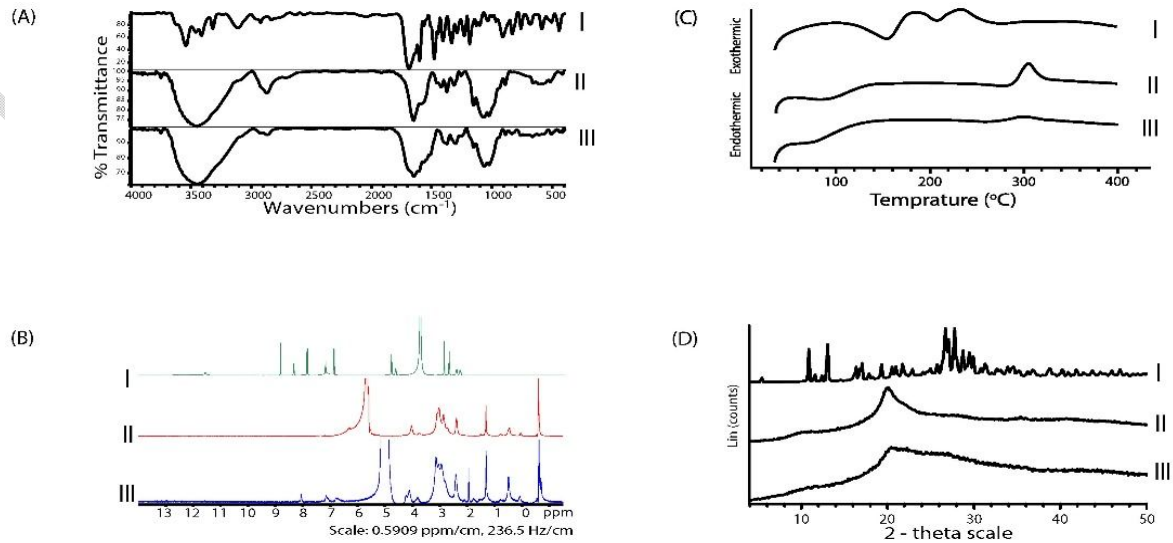

Fig. 2. Characterization of FA-CS conjugate. (A) FTIR spectroscopy, (B) ^{1}H NMR spectroscopy, (C) DSC thermograms, and (D) XRD patterns of (I) FA, (II) CS, and (III) FA-CS conjugate.

3.2 Preparation and Characterization of MTX Loaded NPs

3.2.1 Entrapment Efficiency Percent (EE%)

EE% of uncoated MTX loaded NPs (F1-F9) was influenced by polymer concentration, drug amount and stabilizer concentration. Regarding polymer concentration, EE% was remarkably amplified by increasing polymer weight from 1% to 2% (w/v) at the studied drug polymer weight ratios 1:5 (F1 vs F2) or 1:10 (F4 vs F5), (Table 1). Increasing polymer concentration results in increased viscosity of PLGA organic phase as well as increased diffusional resistance to drug molecules from organic to aqueous phase [15, 50]. Additionally, the anticipated rapid polymer solidification at higher concentration might abridge the diffusion of drug molecules out of the NPs, increasing drug molecules entrapped within the NPs [15]. On the other hand, further enhancement of polymer weight to 4% (w/v) at both drug polymer ratios 1:5 (F3) and 1:10 (F6), resulted in a remarked decrease in EE%. This could be ascribed to limited drug miscibility in specific polymer concentration beyond which no increment in drug entrapment could be seen because free drug molecules in the polymer matrix were driven to those in the aqueous phase [15]. Thus, increasing polymer content might influence drug dispersion in organic phase, besides its impact on drug polymer affinity and/or interaction [51]. It can be concluded that polymer concentration of 2% (w/v) was optimum for maximum drug polymer miscibility in this study. Increment in drug amount at fixed polymer concentrations (F4 vs F1, F5 vs F2, and F6 vs F3) has remarkably increased the drug entrapment due to enhanced interaction between drug and PLGA at higher drug amount [15, 52]. Increasing PVA concentration from 1% to 2% (w/v) drastically diminished the EE%. Higher PVA concentration could enhance the water solubility of MTX as a micelle in the external aqueous phase and could encourage more drug molecules to partition out rapidly and escape from the primary emulsion into the aqueous phase during the emulsification step, leaving fewer drug molecules to interact with PLGA in emulsion droplets [53]. As shown in Table 1, F2 conferred superior physicochemical characteristics (EE% 81.27 ± 1.73, PS 173.7 ± 0.66, PDI 0.139 ± 0.025 and ζP -16.63 ± 0.51) and was chosen for further modification with FA-CS conjugate. EE% of F2 after coating with 0.1% and 0.2% (w/v) FA-CS conjugate (F10 and F11, respectively) (Table 1) was adequate for an optimal targeted nanocarrier. Reduction in EE% of F10 and F11 could be attributed to enhanced dissolution and further reduction in surface adsorbed drug that could happen while surface coating of NPs in conjugation solution [54]. Additionally, part of the encapsulated drug might have dislodged out of the NPs during coating due to interaction between the negative charge of PLGA and the positive charge of CS [33]. Reduction in EE% was statistically nonsignificant after coating in F10 but statistically significant (p<0.05) after coating in F11, so F10 showed augmented EE%.

3.2.2 Particle Size (PS) and Polydispersity Index (PDI)

PS and PDI of the prepared MTX loaded NPs are illustrated in Table 1. Noteworthy, PS was gradually increased as the polymer concentration increased, at both drug polymer weight ratios (1:5 or 1:10) or at fixed drug amounts (F1 vs F5 and F2 vs F6), that might have been caused by an increase in the viscosity of the organic phase, leading to reduction in net shear stress and the formation of larger particles [27, 50]. Moreover, the dispersion rate of PLGA solution in the aqueous phase might have decelerated as the viscosity of the organic phase increased, forming larger droplets, and generating larger NPs as the organic solvent is eliminated [55-57]. Moreover, PS slightly decreased as drug amount increased (F4 vs F1, F5 vs F2, and F6 vs F3) at maintained polymer concentration, which could be related to the fact that at higher drug amount, drug polymer interaction increases [52]; henceforth, polymer-polymer and polymer-solvent interaction diminish and so does the PS as such polymer related interactions impart significant increment in the PS [55]. This correlates directly with results of EE% that increased at higher drug amount due to increased drug polymer interaction. Other researchers found reduction in PS as drug concentration increased [58], while others reported slight reduction in PS upon drug loading in NPs [59]. PS dramatically increased when PVA concentration raised from 1% (w/v) to 2% (w/v), which could be related to increase in the viscosity of the aqueous phase, counteracting the net shear force to break up droplets[60]. In addition, when PVA concentration increases, residual PVA molecules can deposit on the surface of the NPs and coalescence of NPs may be enhanced, increasing PS [60]. Similar results were reported earlier in literature [56]. As shown in Table 1, PS was significantly (p<0.001) increased upon surface modification with FA-CS conjugate (F10 and F11) compared to the selected uncoated formulation (F2), which could be assigned to the electrostatic interaction and hydrogen bonding between the protonated amino groups of CS and negatively charged carboxylate groups of PLGA, confirming efficient surface functionalization of FA-CS on NPs surface, depending on adsorption mechanism [2]. Furthermore, the increment in PS as the concentration of FA-CS increased from 0.1% (F10) to 0.2% (F11) could be explained by deposition of larger amounts of FA-CS conjugate on the surface of PLGA NPs as the concentration of FA-CS increased [61]. It has been reported in literature that maximum uptake and contact with mucosal epithelial membranes were found for polymeric NPs of 50 to 500 nm [12]. Moreover, transcytosis of NPs for gastrointestinal (GI) absorption is more enhanced for NPs with size < 500 nm [62, 63]. Besides, PLGA NPs with size < 500 nm can avoid intestinal wall metabolizing enzymes as well as GI tract P-glycoprotein dependent excretion [63]. Recent findings reported the convenience of oral administration of NPs with size of 350 nm [64]. Considering PS of F10, the prepared targeted MTX nanocarrier was appropriate for oral administration and eligible for transport via the GI tract, thus reaching the systemic circulation. The PDI values of all uncoated MTX NPs ranged from 0.030 ± 0.019 to 0.203 ± 0.036 and from 0.154 ± 0.136 to 0.238 ± 0.018 for FA-CS coated MTX NPs. All prepared formulations had low PDI value (< 0.3), indicating homogenous size distribution and stable colloidal dispersion that is highly monodispersed [65, 66].

3.2.3 Zeta Potential (ζP)

ζP is a pivotal parameter to assess the stability of colloidal dispersion. In fact, ζP values around ±30 mV indicate optimal stability in dispersion medium [12, 51]. As delineated in Table 1, ζP values for all the uncoated MTX NPs formulations ranged between -22.87 ± 1.36 mV and -11.27 ± 0.25 mV. Uncoated MTX NPs are apt to be negatively charged due to the polyanionic nature of PLGA due to terminal carboxylate groups on the surface of NPs [50, 55]. Increase in polymer concentration from 1% to 4% had no clear contribution on ζP. Of noted, formulations prepared at higher drug polymer weight ratio (1:10) exhibited relatively more negative ζP, which might be attributable to availability of a greater number of free carboxylate groups on the surface of NPs [55]. Earlier studies reported ζP dependence on drug polymer ratio [53]. Formulations prepared with higher PVA concentration (F7, F8, and F9) had slightly less negative ζP values than that of those prepared with lower PVA concentration, which might be due to deposition of multiple protective layers of PVA on the surface of PLGA NPs at higher PVA concentration, shielding the negative charge of NPs surfaces [53]. As shown in Table 1, ζP values switched to the positive side, ranging between 34.03 ± 1.68 mV (F10) and 33.37 ± 3.55 mV (F11), after coating with FA-CS due to positive charge of free amino groups carried by FA-CS [9], verifying an efficient modification of the surface of the NPs. Analogous results were previously reported about FA-CS coated PLGA NPs [2, 8]. Notably, increasing concentration of FA-CS did not considerably affect the ζP, which could be related to the saturation of the surface of the NPs with the adsorbed FA-CS conjugate [33]. Moreover, ζP of FA-CS coated NPs F10 and F11 were > 30 mV, confirming their stability. The positive ζP can be advantageous for the prepared targeted nanocarrier by enhancing its attraction and binding to the negatively charged target cells [67], namely FR-overexpressing cells.

Table 1. Characterization of different MTX-loaded NPs

Formula code	Drug polymer ratio	PLGA% (w/v)	PVA (w/v %)	FA-CS (w/v %)	EE%	Particle Size (nm)	PDI	Zeta Potential (mV)
F1	1:5	1	1	-	72.58 ± 1.01	154.9 ± 2.97	0.067 ± 0.043	-18.00 ± 0.36
F2	1:5	2	1	-	81.27 ± 1.73	173.7 ± 0.66	0.139 ± 0.025	-16.63 ± 0.51
F3	1:5	4	1	-	69.24 ± 1.08	188.8 ± 2.48	0.057 ± 0.034	-17.87 ± 1.14
F4	1:10	1	1	-	68.33 ± 1.11	169.7 ± 2.10	0.203 ± 0.036	-22.87 ± 1.36
F5	1:10	2	1	-	75.35 ± 3.28	185.6 ± 1.10	0.092 ± 0.024	-21.93 ± 0.86
F6	1:10	4	1	-	61.09 ± 1.91	196.1 ± 2.69	0.101 ± 0.007	-22.7 ± 2.12
F7	1:5	1	2	-	65.35 ± 1.53	206.4 ± 1.77	0.063 ± 0.018	-17.23 ± 2.73
F8	1:5	2	2	-	73.92 ± 0.64	216.1 ± 1.85	0.153 ± 0.067	-15.33 ± 0.42
F9	1:5	4	2	-	69.44 ± 1.42	223.9 ± 2.91	0.030 ± 0.019	-11.27 ± 0.25
F10	1:5	2	1	0.1	76.23 ± 3.39	278.6 ± 22.17***	0.238 ± 0.018	34.03 ± 1.68
F11	1:5	2	1	0.2	72.90 ± 1.31*	352.9 ± 7.13***	0.154 ± 0.136	33.37 ± 3.55

*Data are expressed as mean ± SD (n = 3). Statistical significances are indicated as *p<0.05 and ***p<0.001 vs optimal uncoated MTX NPs (F2).*

3.2.4 *In Vitro* Release Studies and Kinetics Analysis

MTX release profile from the selected uncoated formulation (F2) and from both FA-CS coated formulations (F10 and F11) in comparison with free MTX is illustrated in Figure 3. Free MTX exhibited complete liberation in the first 3 h in pH 6.8 and 7.4 (Figure 3(B,C)), respectively, which was similarly mentioned in earlier findings [21, 68]. However, less free MTX was released at acidic pH (1.2) at the first 3 h and extended over 8 h (Figure 3(A)), owing to the weak acidity of MTX (pKa values: 3.8, 4.8, and 5.6) [69]; thus it is more soluble in neutral pH than in acidic media. These results were in unison with earlier reports [70]. MTX release from uncoated (F2) and FA-CS coated (F10 and F11) displayed a biphasic behavior, an initial burst release in different media for the first 2 h followed by sustained release up to 8 h. The initial burst release could be accredited to MTX molecules existing near the surface of the NPs [35] or loosely attached in the NPs [61], along with the accelerated diffusion of release medium into NPs due to their large surface area [15]. Furthermore, MTX encapsulated in the inner core of the polymeric matrix was responsible for the sustained release behavior from 2 to 8 h because of the biodegradation of the polymeric matrix and slow drug diffusion from such matrix [61]. FA-CS coated (F10 and F11) showed significantly lower cumulative amount released at 2 h and 8 h than that of uncoated (F2) in all release media, indicating that coating with FA-CS conjugate could act as an additional physical barrier to hinder drug desorption and diffusion to the bulk solution [11]. Additionally, the decreased MTX release from FA-CS coated (F10 and F11) was more pronounced in pH 6.8. Given that CS has pKa of 6.3 due to free amino groups, these amino groups will be deprotonated and uncharged when the pH increase above 6.3, forming insoluble polymer shell and lowering MTX release from FA-CS coated formulations (F10 and F11), while, in lower pH, stronger protonation of the amino groups and more dissolution of CS in release media occurs, creating more loose NPs and decreasing the coating layers around the NPs [9, 71]. MTX release was accelerated at pH 7.4, owing to the heterogeneous PLGA degradation at such pH [48]. Such observations confirmed that the surface of the MTX NPs formulation was modified after coating with FA-CS conjugate. It can be concluded that FA-CS coated (F10 and F11) acted as controlled drug delivery systems. Therefore, F10 was chosen as the optimized FA-CS coated formulation based on presence of no significant variation in drug release patterns between F10 and F11, besides F11 showed significant (p<0.05) decline in EE% of MTX compared to the selected uncoated formulation (F2).

According to the values of R^2 depicted in Table 2, it can be deduced that all studied formulation followed Higuchi diffusion model regardless of the pH of the release medium. Additionally, the n values of the Korsmeyer-Peppas model revealed that MTX release at all media from F2 was non-Fickian transport that the mechanism of release was a mixture of drug diffusion and polymeric matrix erosion, while its release from F10 and F11 in pH 1.2 and 6.8 was Fickian, which substantially governed by diffusion from polymeric matrix, while in pH 7.4, MTX release from FA-CS coated MTX NPs followed non-Fickian transport.

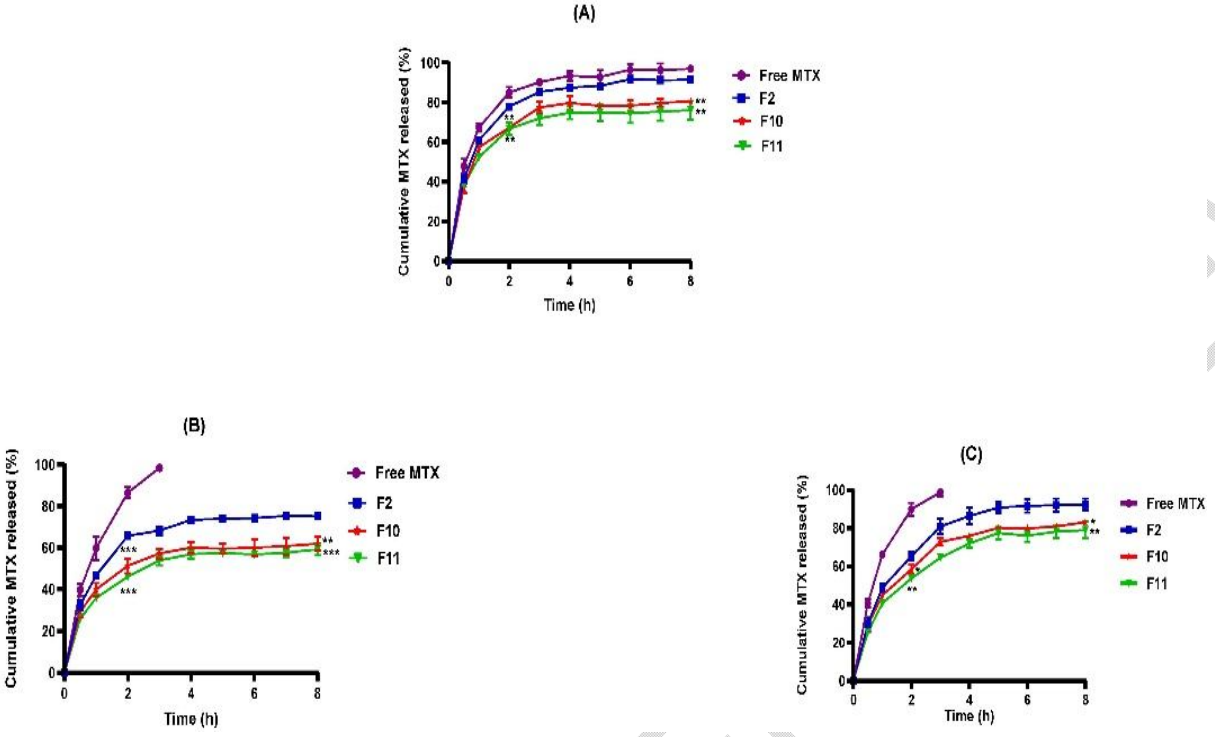

Fig 3. *In vitro* release of MTX at (A) pH 1.2, (B) pH 6.8, and (C) pH 7.4.
Each point represents the mean ± SD (n = 3). Statistical significances are indicated as $^{*}p<0.05$, $^{**}p<0.01$, and $^{***}p<0.001$ vs optimal uncoated MTX NPs (F2).

Table 2. *In vitro* MTX release data kinetics analysis

Formula code	pH of the release media	Coefficient of determination (R^2)			Korsmeyer-Peppas		Main transport mechanism
		Zero order	First order	Higuchi model	(R^2)	Diffusional exponent (n)	
Uncoated MTX NPs (F2)	1.2	0.6103	0.8354	0.8454	0.9739	0.5697	Non Fickian diffusion
	6.8	0.6221	0.7425	0.8523	0.9795	0.5100	Non Fickian diffusion
	7.4	0.7335	0.8636	0.9195	0.9396	0.5752	Non Fickian diffusion
FA-CS coated MTX NPs (F10)	1.2	0.5719	0.6957	0.8128	0.8980	0.4359	Fickian diffusion
	6.8	0.6027	0.6840	0.8341	0.9418	0.3537	Fickian diffusion
	7.4	0.7270	0.8695	0.9197	0.9620	0.5014	Non Fickian diffusion
	1.2	0.5594	0.6643	0.8020	0.9735	0.4023	Fickian diffusion

FA-CS coated MTX NPs (F11)	6.8	0.6468	0.7255	0.8694	0.9113	0.2900	Fickian diffusion
	7.4	0.7621	0.8662	0.9370	0.9822	0.5118	Non Fickian diffusion

3.2.5 Fourier Transform Infrared Spectroscopy (FTIR)

FTIR spectroscopy, Figure 4(A), was employed to encounter the likelihood of any physicochemical interactions among the NPs components and asses their compatablility [55]. The spectrum of MTX (I) revealed absorption peaks at 3420, 2955, 1647, 1603, 1497, 1406, and 1208 cm^{-1} corresponding to N–H stretching vibration, C–H stretching, C=O functional group from amide I, amide II band resulting from NH_2 bending along with C-N stretching, aryl system, C-O group, together with C=O moiety and amide III band, respectively [72]. PLGA spectrum (II) exhibited the characteristic peaks at 3528 and 1747 cm^{-1} attained to the stretching vibration of –OH and C=O, respectively, of its monomers, lactide and glycolide [35]. The symmetric stretching of –CH, $–CH_2$ and $–CH_3$ was distinguished by two absorption bands at 2883 and 2955 cm^{-1}, while the asymmetric stretching of $–CH_3$ and $–CH_2$ were characterized by distinct peaks at 1398 and 1459 cm^{-1}. Bands around 1085 -1186 cm^{-1} were correlated to stretching vibration of C–O [35, 73]. PVA spectrum (III) displayed discriminative bands at 3422, 2940, 1736, 1098 and 850 cm^{-1} due to stretching vibrations of –OH, C–H, C=O, C–O, and C-C groups of PVA, respectively [35, 74]. The spectrum of FA-CS (IV) showed the distinguished peak at 3451cm^{-1} attributed to the overlapping between NH- and OH- groups of FA and CS [25], together with amide (CONH-) peak at 1654 cm^{-1} that was attributed to the interaction between the amino group of CS with the carboxylate group of FA [42, 43] and NH bending in the second amine group at 1570 cm^{-1} [25, 45, 46]. The spectrum of physical mixture (V) corresponding to FA-CS coated MTX NPs (F10) represented peaks of each component with abscense of the peaks of FA-CS due to diluton effect [33], with no additional peaks, eliminating the likelihood of interactions among the components. Spectrum of the optimized FA-CS coated MTX NPs (F10) (VII) coincided with that of its plain NPs (VI) and showed the characteristics peak of MTX at 1650 cm^{-1}, suggesting MTX molecules were loaded in/on the polymeric matrix [75] and negating interaction between MTX and NPs ingredients [65]. Moreover, the spectra of F10 and its plain NPs showed the characteristic band of FA-CS at 3451 cm^{-1}, confirming efficient coating with FA-CS conjugate [9].

3.2.6 Differential Scanning Calorimetry (DSC)

As explicated in Figure 4(B), the crystalline nature of pure MTX (I) was indicated by the presence of melting endothermic peak at 93.3 - 123.4°C [72]. Thermograms of PLGA and PVA, (II and III, respectively), did not reveal any sharp melting points; instead PLGA showed endotherms at 45.5°C and 360.6°C which related to its glass transition temperaure [76] and decomposition [15], respectively, while peaks at 196.9°C and 330.6°C in thermogram of PVA were referred to its melting point and structural degradation, respectively [35]. Thermogram of FA-CS (IV) showed no sharp melting point but showed peaks at 79.7°C and 266°C, which attained to FA-CS conjugation [8]. The characterisic peaks of components of the optimized FA-CS coated MTX NPs (F10) were present in the thermogram of its physical mixture (V), revoking their interaction. It is worth to mention that the endothermic peak of PLGA was shifted to lower temperature in physical mixture themogram, appearing at 303.4°C, which could be ascribed to dissolvation of the polymer in molten MTX [15]. In addition, peak of MTX was shown but with declined intensity and peaks of FA-CS were abscent due to diluton effect [33]. Interestingly, thermogram of F10 (VII) was identical to that of its corresponding plain one (VI), with the disappearance of the endothermic peak of MTX, indicating its encapsulation in the amorphous form inside the polymeric matrix of the formulated NPs [76].

3.2.7 X-Ray Diffractometry (XRD)

XRD is a pivotal approach in scrutinizing the crystallinity of pure drug and formulations, thus utilized in identification of the influence of formulation processing on crystal polymorphism [33]. As shown in Figure 4(C), diffractogram of MTX (I) displayed various diffraction peaks at 2θ region of 7.75°, 9.31°, 11.49°, 13.38°, 19.50°, 23.52°, and 28.94°, indicating its crystallinity [37, 77]. The absence of distinct diffraction peaks in diffractogram of PLGA (II) confirmed its amorphous nature [9, 16], whereas PVA (III) was estimated to have semi-crystalline nature due to presence of broad diffraction peak at 2θ in the range of 19.56° – 22.59° emerging from intramolecular and intermolecular hydrogen bonds between its -OH groups [35], while diffractogram of FA-CS (IV) displayed only a hump peak at 2θ of 20.56°, indicating its declined crystallinity [7, 25]. XRD patterns of the physical mixture of the optimized FA-CS coated MTX NPs (F10) (V) showed the combined patterns of all ingredients, while those of MTX were not vividly shown, owing to dilution effect. The diffractogram of F10 (VII) was in unison with that of its corresponding plain NPs (VI), with diminished number and intensity of peaks of MTX, indicating significant loss of drug crystallinity and its incorporation in the polymeric matrix in the amorphous form [9, 76, 78]. The results of FTIR, along with those of DSC and XRD, go parallel to the same conclusion of the absence of any interaction in the prepared NPs and reduction of MTX crystallinity and its encapsulation in the polymeric matrix of the formulated targeted nanocarrier in the amorphous form.

3.3 Transmission Electron Microscopy (TEM)

TEM photographs of the selected uncoated MTX NPs (F2) and optimal FA-CS coated MTX NPs (F10) (Figure 5) revealed spherical morphology with smooth surfaces. Unlike F2, F10 exhibited clearly obvious dark core surrounded by a faded gray halo, which could be related to FA-CS conjugate coating on the NPs surface. Of interest, NPs exhibited smaller PS when estimated by TEM than that obtained via DLS technique, which can be attributed to the drying effect of polymeric NPs dispersion on a grid during TEM imaging,

omitting influence of surface ions or solvent molecules, in contrast to hydrated state of polymeric NPs that includes double solvation layer during size measurement via DLS. Similar findings were mentioned in literature for PLGA NPs [48, 63].

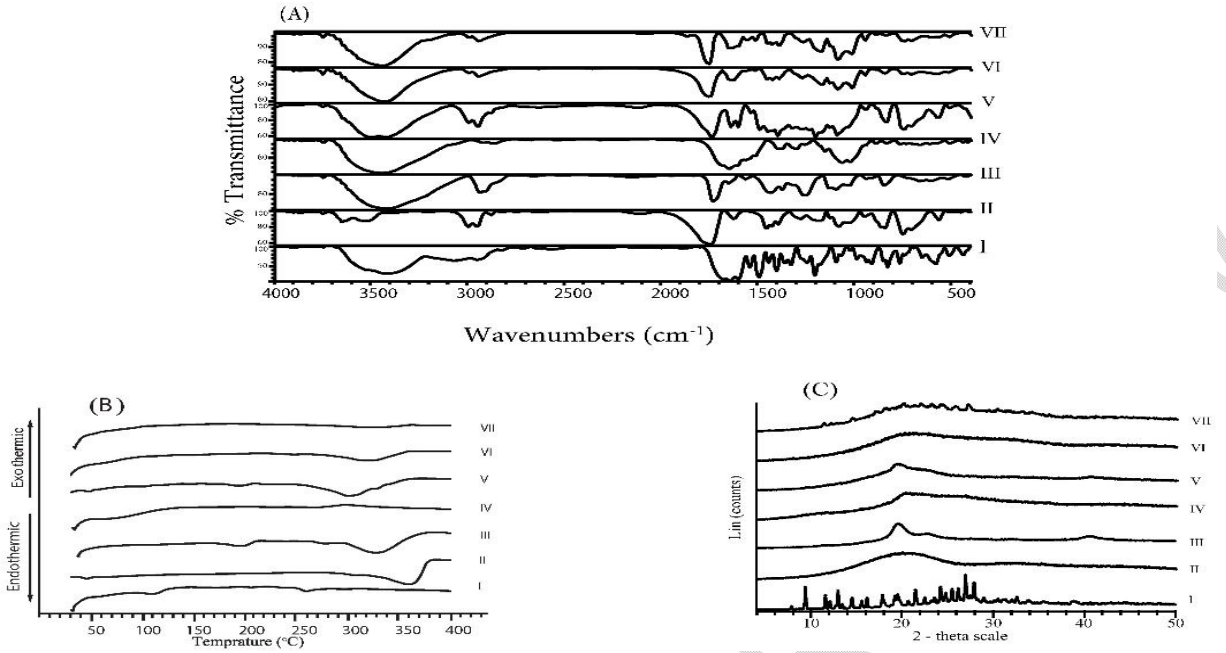

Fig. 4. (A) FTIR spectra, (B) DSC thermograms, and (C) XRD patterns of (I) MTX, (II) PLGA, (III) PVA, (IV) FA-CS, (V) physical mixture of components of FA-CS coated MTX NPs (F10), (VI) plain FA-CS coated NPs, and (VII) the optimized FA-CS coated MTX NPs (F10).

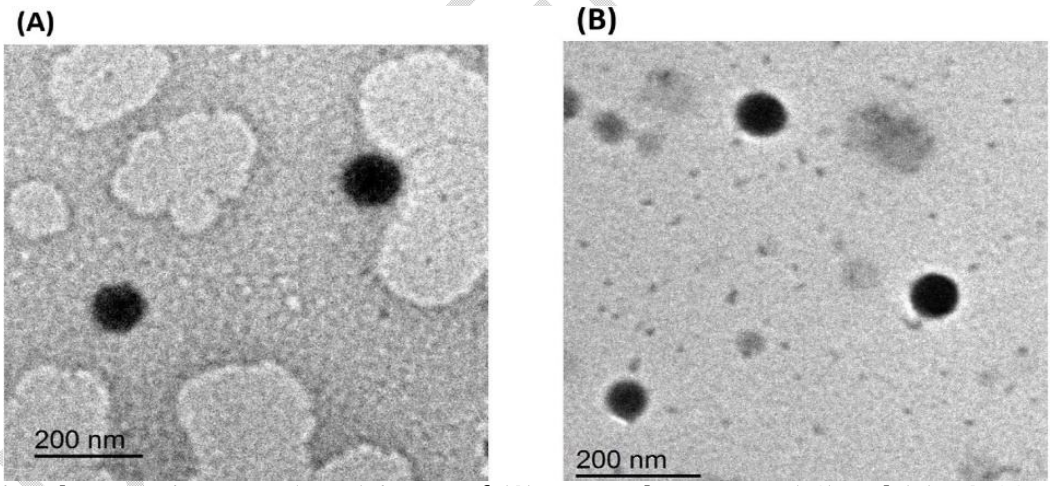

Fig. 5. Transmission electron microscopy (TEM) images of (A) uncoated MTX NPs (F2) and (B) FA-CS coated MTX NPs (F10).

3.4 *In Vitro* Cytotoxicity Assay

The cytotoxicity and antitumor activity of the optimized FA-CS coated MTX NPs formulation (F10) was evaluated and compared to free MTX and uncoated MTX NPs (F2) in both FR-positive MCF-7 [3, 79] and HeLa [13, 80] and FR-negative A549 cells [1, 46] based on MTT assay. Plain NPs showed elevated cell survival rates in all cell lines, Figure 6(A); however, pronounced reduction in cell viability was seen at higher NPs concentration (500 µg/mL). However, IC_{50} values for both plain NPs were more than 140 µg/mL, as shown in Table 3, indicating the safety of the components of the formulated targeted nanocarrier on tested cells. These results agreed with previously mentioned findings in literature [21]. Free MTX, uncoated MTX NPs (F2) and FA-CS coated MTX NPs formulation (F10) caused a remarkable decline in cell viability in a dose-dependent manner in MCF-7 and HeLa cell lines, shown in Figure 6(B). Intriguingly, FA-CS coated MTX NPs (F10) showed enhanced cytotoxicity than free MTX and uncoated MTX NPs (F2) at the same doses on FR-positive cells. IC50 values of FA-CS coated MTX NPs (F10) in MCF-7 and HeLa cells were lower than those of free MTX and uncoated MTX NPs (F2), Table 3. The escalated cytotoxicity of FA-CS coated MTX NPs formulation (F10) in FR-positive cells over free MTX and uncoated MTX NPs (F2) could be attributed to enhanced internalization and uptake of the prepared

FA-decorated nanocarrier through FR-mediated endocytosis (active targeting) as well as passive targeting through the enhanced permeability and retention (EPR) effect due to formation of endothelial gaps up to 500 nm in tumor cells allowing accumulation and permeation of particles of size < 500 nm[46], collectively enhancing cytotoxicity and antitumor effect of MTX. Interestingly, the majority of studies using MTX loaded NPs focus on breast cancer cells [10, 21, 28]. Our findings on HeLa cells could support recent findings reported in literature that MTX could be used to treat cervical cancer in clinical setting [80]. On the other hand, FA-CS coated MTX NPs (F10) did not display enhanced cytotoxicity on A549 cells compared to free MTX, as seen in Figure 6(B); however, FA-CS coated MTX NPs (F10) caused a pronounced increase in % cell viability compared to free MTX at different studied concentrations and exhibited nearly similar cell survival rates to uncoated MTX NPs (F2). A549 cells were less sensitive to FA-CS coated MTX NPs (F10) compared to both studied FR-positive cells, which could be attributed to lack of FR, validating the active targeted delivery of the fabricated FA-CS coated MTX NPs formulation (F10) to FR-positive cells and spotting the light on the role of surface decoration of nanocarrier with FA as a targeting ligand in enhancing the specific and selective uptake by FR-mediated endocytosis. These results were in agreement with recent report in literature [81]. In other words, the augmented antitumor effect of MTX when encapsulated in the prepared nanocarrier (lower IC50) could eventually result in lower dose requirement of FA-CS coated MTX NPs (F10) than that of free MTX for similar efficacy, enhancing MTX safety profile and minimizing its systemic toxicity. Thus, the prepared FA-functionalized nanocarrier could inaugurate a new platform for the targeted delivery of MTX to FR-overexpressing cancer cells and could provide promising outcomes in further pre-clinical studies. *In vivo* evaluation of the therapeutic efficacy of the prepared nanocarrier in treatment of FR-positive tumors upon oral administration is suggested for further investigations.

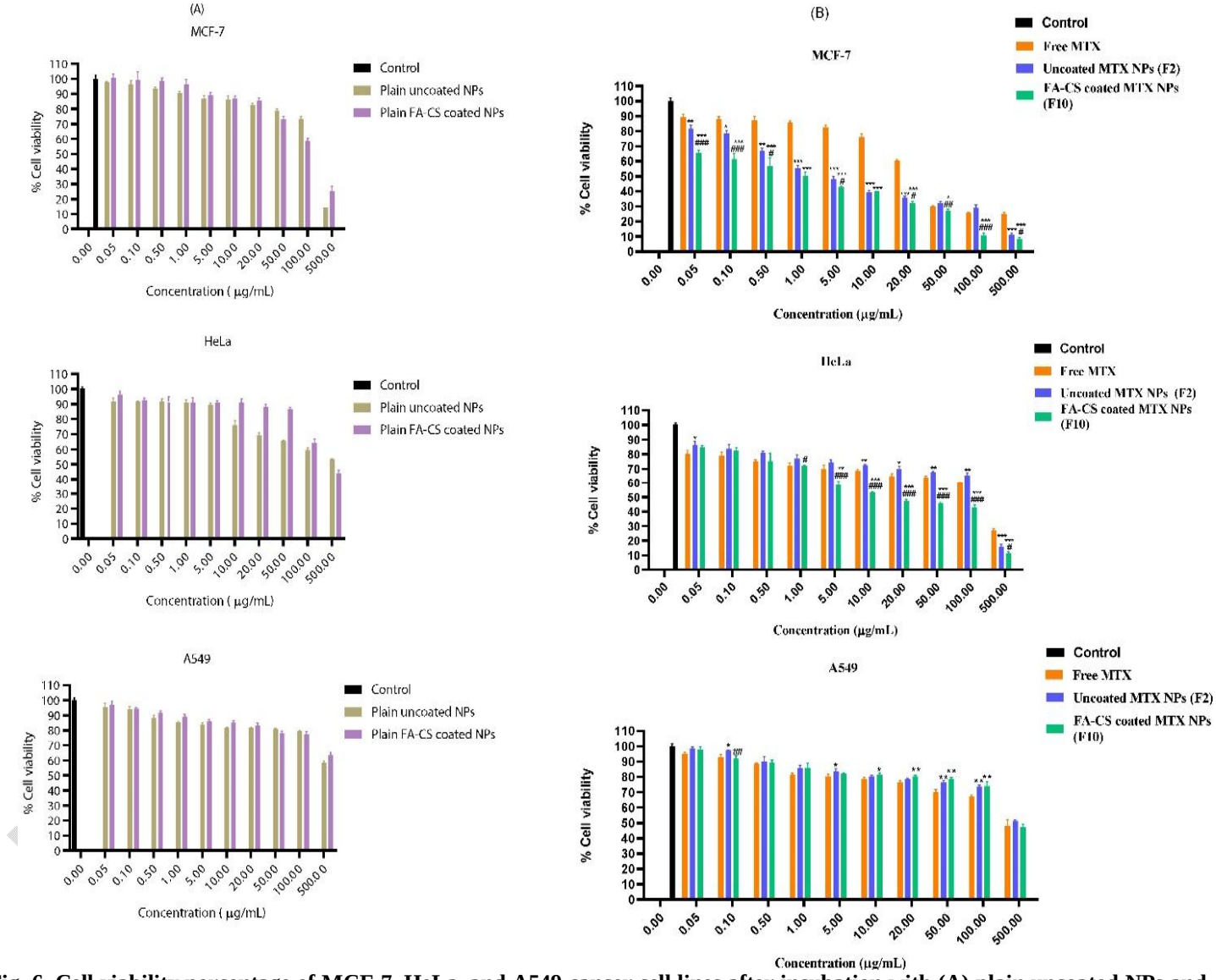

Fig. 6. Cell viability percentage of MCF-7, HeLa, and A549 cancer cell lines after incubation with (A) plain uncoated NPs and plain FA-CS coated NPs and (B) free MTX, uncoated MTX NPs (F2), and FA-CS coated MTX NPs (F10) after 24 hours.

Data are represented as mean ± SD (n = 3). Statistical significances are indicated as $^{*}p<0.05$, $^{**}p<0.01$, and $^{***}p<0.001$ vs free MTX, and $^{\#}p<0.05$, $^{\#\#}p<0.01$ and $^{\#\#\#}p<0.001$ vs uncoated MTX NPs (F2).

Table 3. The obtained half inhibitory concentration (IC50) values during MTT assay to folate receptor-positive MCF-7 and HeLa cancer cell lines after incubation for 24 hours.

Tested formula	IC50 (µg/mL)	
	MCF-7	HeLa
Free MTX	30.35	154.5
Plain uncoated NPs	>140	>140
Uncoated MTX NPs (F2)	3.51	122.9
Plain FA-CS coated NPs	>140	>140
FA-CS coated MTX NPs (F10)	0.91	15.49

3.5 Storage Stability Study

The optimized FA-CS coated MTX NPs (F10) presented adequate physical stability at ambient or refrigerated temperature. F10 did not exhibit any change in color or odor with no signs of phase separation over the period of 3 months. The results depicted in Table 4 outlined that F10 was stable at refrigerator storage temperature over the whole period with nonsignificant differences noticed in all parameters when compared to the initial values obtained once F10 was freshly prepared. On the other hand, there was a statistically significant increase in PS (p<0.01) and PDI (p<0.05) values of F10 only after 3 months and significant decrease in EE% (p<0.05) upon storage at ambient temperature, while ζP values did not display any marked change. PS increase could be attained to particles collision [34]. Therefore, the formulated FA-decorated nanocarrier was considerably stable at refrigerator temperature with dominance of homogenously distributed nanosized particles. Analogous outcomes of storage stability study of FA-CS coated PLGA NPs were published earlier [8].

Table 4. Storage stability assessment parameters of optimal FA-CS coated MTX NPs (F10) suspension at ambient temperature and refrigerated temperature over three months.

Storage time	Evaluation parameters							
	Ambient temperature				Refrigerated temperature (4 ± 1°C)			
	EE%	Particle size (nm)	PDI	Zeta Potential (mV)	EE%	Particle size (nm)	PDI	Zeta Potential (mV)
Zero time	79.3 ± 0.9	286.9 ± 10.5	0.21 ± 0.03	33.4 ± 2.3	79.3 ± 0.9	286.9 ± 10.5	0.21 ± 0.03	33.4 ± 2.3
1 month	76.6 ± 2.6	309.1 ± 15.7	0.22 ± 0.13	32.9 ± 3.2	83.0 ± 2.2	288.8 ± 28.2	0.29 ± 0.07	36.4 ± 9.1
2 months	78.0 ± 0.7	265.7 ± 4.1	0.26 ± 0.04	41.3 ± 3.7	80.8 ± 1.8	269.3 ± 4.1	0.26 ± 0.02	26.4 ± 4.3
3 months	74.0 ± 1.2*	337.1 ± 8.1**	0.5 ± 0.19*	39.4 ± 3.5	77.5 ± 2.8	275.8 ± 11.8	0.30 ± 0.03	39.5 ± 1.9

*Data are represented as mean ± SD (n = 3). *p<0.05 and **p<0.01 monthly vs initial measurement.*

3.6 *In Vivo* Evaluation of Therapeutic Efficacy and Safety

3.6.1 Assessment of Arthritis Macroscopical Changes and Serum Rheumatoid Factor (RF) Levels

The optimum targeted FA-CS coated MTX NPs formulation (F10), along with pure MTX, commercial MTX tablets, and plain FA-CS coated NPs formulation, were orally administered to CFA-induced RA mice. CFA-induced RA group exhibited significant (p<0.001)

elevation in arthritis index and paw thickness compared to normal control group in week 5 and on day 32, respectively, indicating a well-established RA model, as shown in Figure 7(B,D), respectively. Noteworthy, FA-CS coated MTX NPs (F10), pure MTX, and commercial MTX tablets orally treated groups exhibited considerable inhibition of RA symptoms compared to CFA-induced RA group, with ~ 85%, 80%, and 60% reduction in arthritis index and ~ 27%, 23.6%, and 13.5% reduction in paw thickness, respectively. Intriguingly, oral treatment with FA-CS coated MTX NPs formulation (F10) exhibited significant decrease in arthritis index (p<0.001) and in paw thickness (p<0.01) compared to treatment with commercial MTX tablets. Additionally, arthritis changes of RA were normalized in FA-CS coated MTX NPs (F10) treated group by the end of the treatment protocoal, emphasizing the potentiated therapeutic performance of the prepared MTX targeted nanocarrier over pure MTX and commercial MTX tablets. The right hind paw photographs and radiographs of all groups included in the study were shown in Figure 7(E,F), respectively. It is crystal clear that the paw photograph of FA-CS coated MTX NPs (F10) orally treated group was comparable to that of the control group. Furthermore, radiographic examination of the joints of FA-CS coated MTX NPs (F10) orally treated mice revealed pronounced reduction in the manifestations of RA compared to CFA-induced RA group that showed severe arthritis in the form of marginal osteophytes and sclerosis of the articular surfaces with relative narrowing of the medial and lateral joint compartment, which was an additional indicator consistent with the previous results. CFA-induced RA group showed a significant (p<0.001) increase in serum RF levels compared to that of the normal control group, as depicted in Figure 7(G). On the other hand, treatment with MTX in all groups signifiacntly (p<0.001) decreased serum RF levels compared to that of CFA-induced RA group, while those in both pure MTX and FA-CS coated MTX NPs (F10) orally treated groups were normalized. FA-CS coated MTX NPs (F10) group displayed significant (p<0.05) reduction in serum RF levels compared to commercial MTX tablet orally treated group, validating the potency of the prepared targeted MTX nanocarrier in the oral treatment of RA compared to conventional MTX tablets preparation.

Fig. 7. Therapeutic efficacy of FA-CS coated MTX NPs (F10) on CFA-induced RA model in mice. (A)The weekly arthritis index of mice in all experimental groups. (B) Arthritis index in the 5th week in all experimental groups. (C) Hind paw thickness measurements of all experimental groups over the study period. (D) Hind paw thickness of all experimental groups on day 32. (E) Macroscopic photographs and (F) X-ray radiographs of affected hind paws of mice in (I) Normal control group, (II) CFA-induced RA group, (III) pure MTX, (IV) commercial MTX tablets, (V) plain FA-CS coated NPs, and (VI) FA-CS coated MTX NPs (F10) orally treated groups. (G) Serum rheumatoid factor (RF) levels.

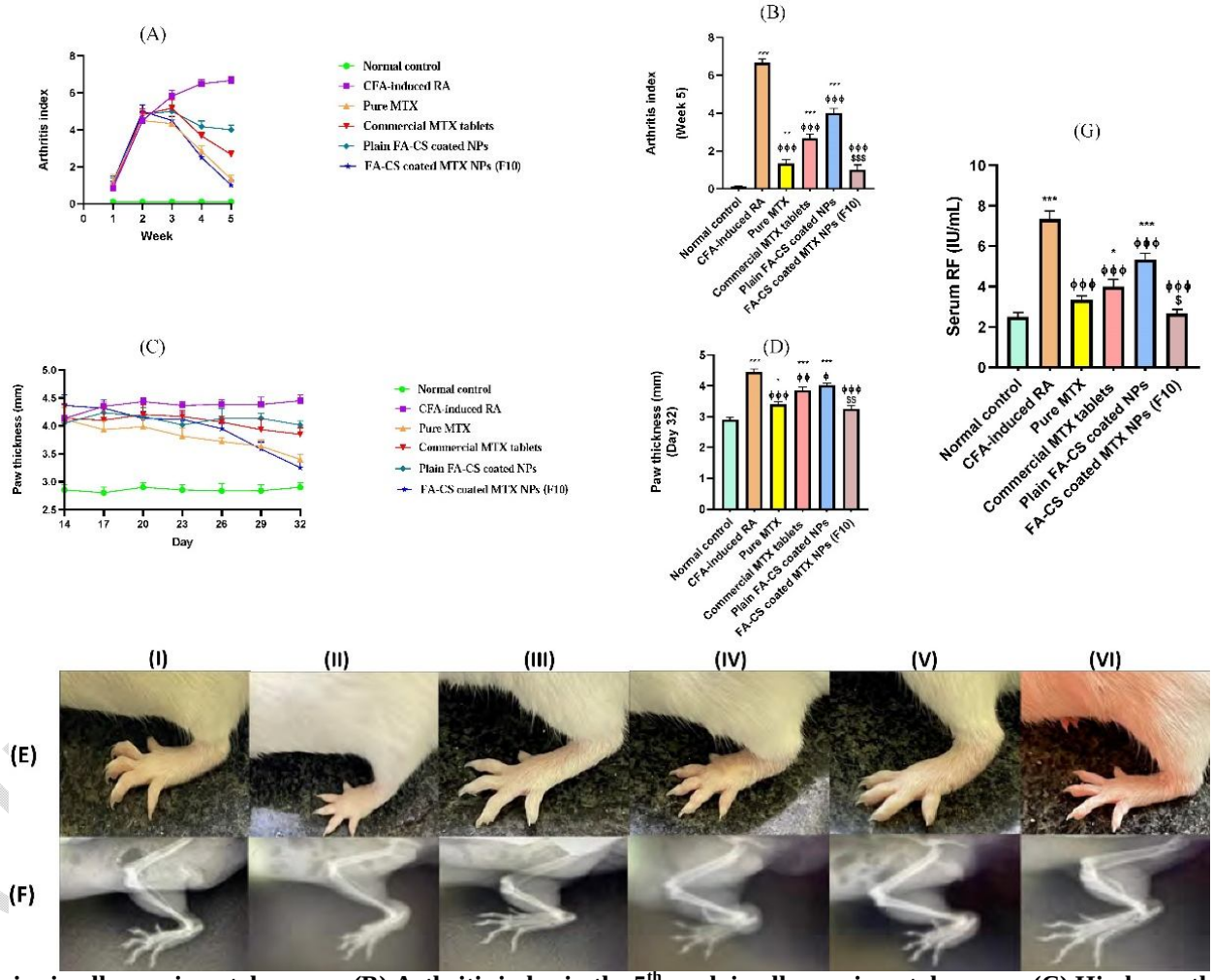

Data are expressed as the mean ± SEM (n = 6). Statistical significances are indicated as $^{*}p<0.05$, $^{**}p<0.01$, and $^{***}p<0.001$ vs normal control group, $^{\phi}p<0.05$, $^{\phi\phi}p<0.01$, and $^{\phi\phi\phi}p<0.001$ vs CFA-induced RA group, $^{\$}p<0.05$, $^{\$\$}p<0.01$, and $^{\$\$\$}p<0.001$ vs commercial MTX tablets treated group.

3.6.2 Determination of Pro-inflammatory Cytokines

In RA, some pro-inflammatory cytokines secreted by macrophages, namely TNF-α, IL-1β, and IL-6, are fundamental pathophysiological elements that provoke a cascade of cytokines responsible for chronic inflammatory response and progression of RA [36, 82], along with osteoclasts activation, resulting in bone destruction and damage [17], which may broaden and expand to subchondral and periarticular soft tissues leading to lethal irreversible disabilities [83].

RA progression in mice was confirmed by a significant (p<0.001) elevation in paw tissue levels of TNF-α, IL-1β, and IL-6 in CFA-induced RA group compared to normal control, as illustrated in Figure 8. Compared to CFA-induced RA group, all the orally treated groups exhibited a significant (p<0.001) decline in all cytokines levels. Mice in FA-CS coated MTX NPs (F10) orally treated group displayed significantly lower levels of TNF-α (p<0.01), IL-1β and IL-6 (p<0.05) compared to pure MTX and significantly (p<0.001) lower levels of all cytokines compared to commercial MTX tablets orally treated groups. The cytokines levels in pure MTX and commercial MTX tablets groups were approximately 1.4 and 1.6 times higher for TNF-α, 1.3 and 1.5 times more in IL-1β, and 1.4 and 1.8 times more in IL-6 than those of FA-CS coated MTX NPs (F10) group, respectively. In addition, TNF-α and IL-6 levels were restored to their normal levels after oral treatment with FA-CS MTX NPs (F10), proving the potentiated efficacy of the formulated targeted MTX nanocarrier in slowing down the progression of RA compared to conventional MTX delivery systems. Notably, plain FA-CS coated NPs orally treated mice demonstrated significant (p<0.001) reduction in levels of all paw homogenate pro-inflammatory cytokines compared to the untreated group.

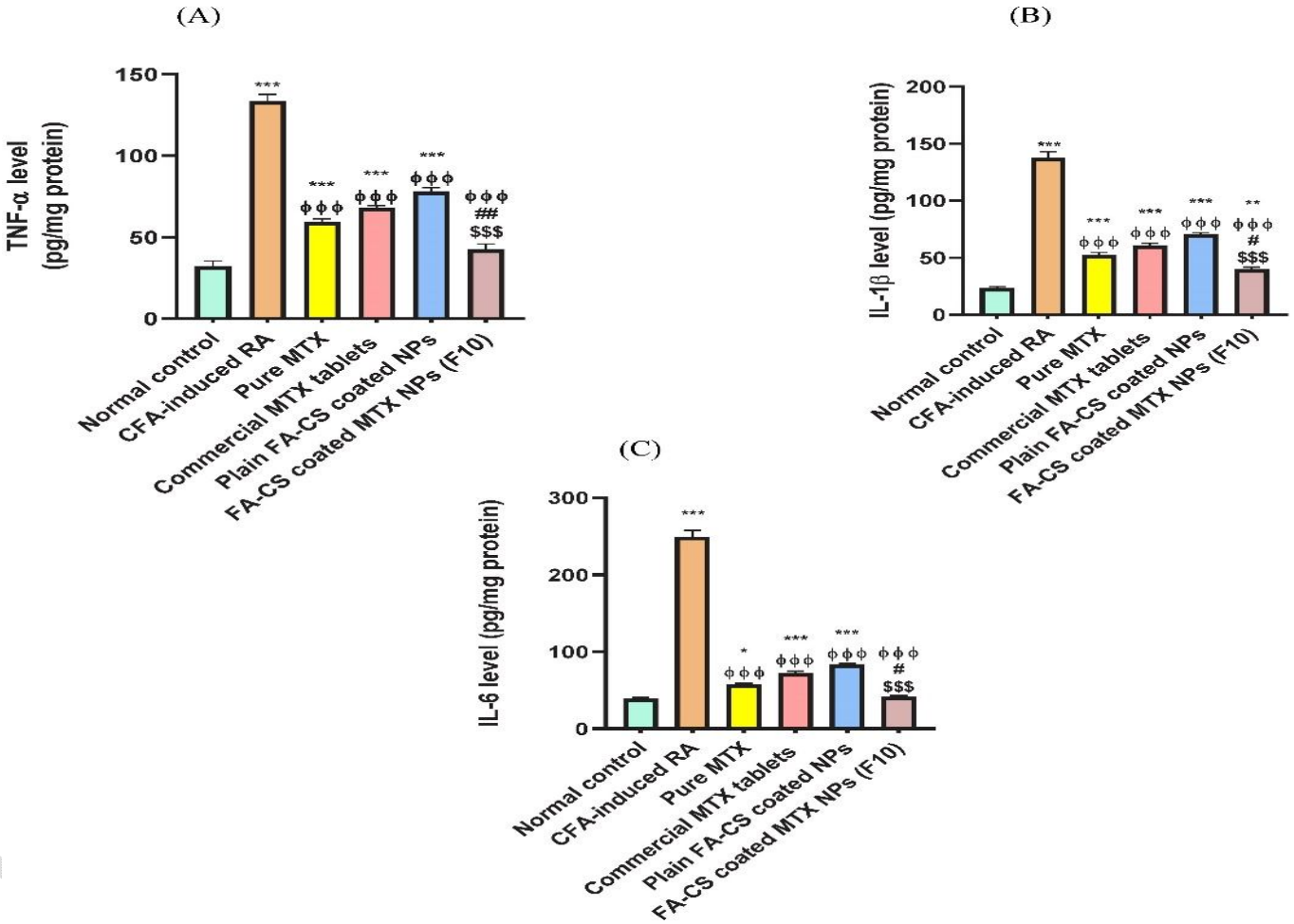

Fig. 8. Impact of the inspected formulations on CFA-induced changes in levels of pro-inflammatory cytokines (A) TNF-α, (B) IL-1β and (C) IL-6 in paw homogenate of mice in different experimental groups.

Data are represented as the mean ± SEM (n = 6). Statistical significances are indicated as $^{*}p<0.05$, $^{**}p<0.01$, and $^{***}p<0.001$ vs normal control group, $^{\phi\phi\phi}p<0.001$ vs CFA-induced RA group, $^{\#}p<0.05$ and $^{\#\#}p<0.01$ vs pure MTX treated group, and $^{\$\$\$}p<0.001$ vs commercial MTX tablets treated group.

3.6.3 Histopathological Analysis of Paw

Microphotographs of H&E-stained sections of paw bone, cartilaginous structure, and synovial membrane are depicted in Figure 9(a) and paw soft tissue from all experimental groups are shown Figure 9(b).The normal control group sections revealed normal joint

cavity, normal structure of the bone cortex lamellae and bone marrow cavity and normal structure of epidermis and subcutaneous tissue. On the contrary, CFA-induced RA group showed extensive hyperplasia of synovial membrane with inflammatory cell infiltration, disrupted bone lamella, and dilated bone marrow cavity, together with severe inflammatory affection of epidermis in the form of hyperkeratosis and epithelial proliferation. The subcutaneous tissue showed marked edema with diffused inflammatory cell infiltrations. Pure MTX and commercial MTX tablets orally treated groups showed less marked disrupted bone lamellae and bone cavity, while the former exhibited improved joint cavity with mild inflammatory cell infiltration and the latter showed evident pannus formation. Pure MTX and commercial MTX tablets showed noted improvements in the affections of the subcutaneous tissue seen in the CFA-induced RA group.

Similar findings to those in the aforementioned CFA-induced RA group were seen in the plain FA-CS coated NPs orally treated group but with slightly lesser extent. Interestingly, oral treatment with FA-CS MTX NPs (F10) exhibited the most obvious alleviation of the destructive manifestations of RA shown in diseased group, with almost normal joint cavity, minimal affection of the cortical bone lamellae, minimal affection of the epidermis without any remarked hyperkeratosis or epithelial proliferation, minimal edema, and scarce inflammatory cell infiltration in subcutaneous tissue. Accordingly, FA-CS coated MTX NPs (F10) treated group had the least histopathological score that was significantly decreased compared to CFA-induced RA group ($p<0.001$), pure MTX treated group ($p<0.05$) and commercial MTX tablets treated group ($p<0.001$), Figure 9(c). Substantially, the histopathological investigations were in agreement with the results of pro-inflammatory cytokines levels in different experimental groups, a validation of the enhanced therapeutic benefits of oral administration of the investigated MTX nanocarrier in treatment of RA.

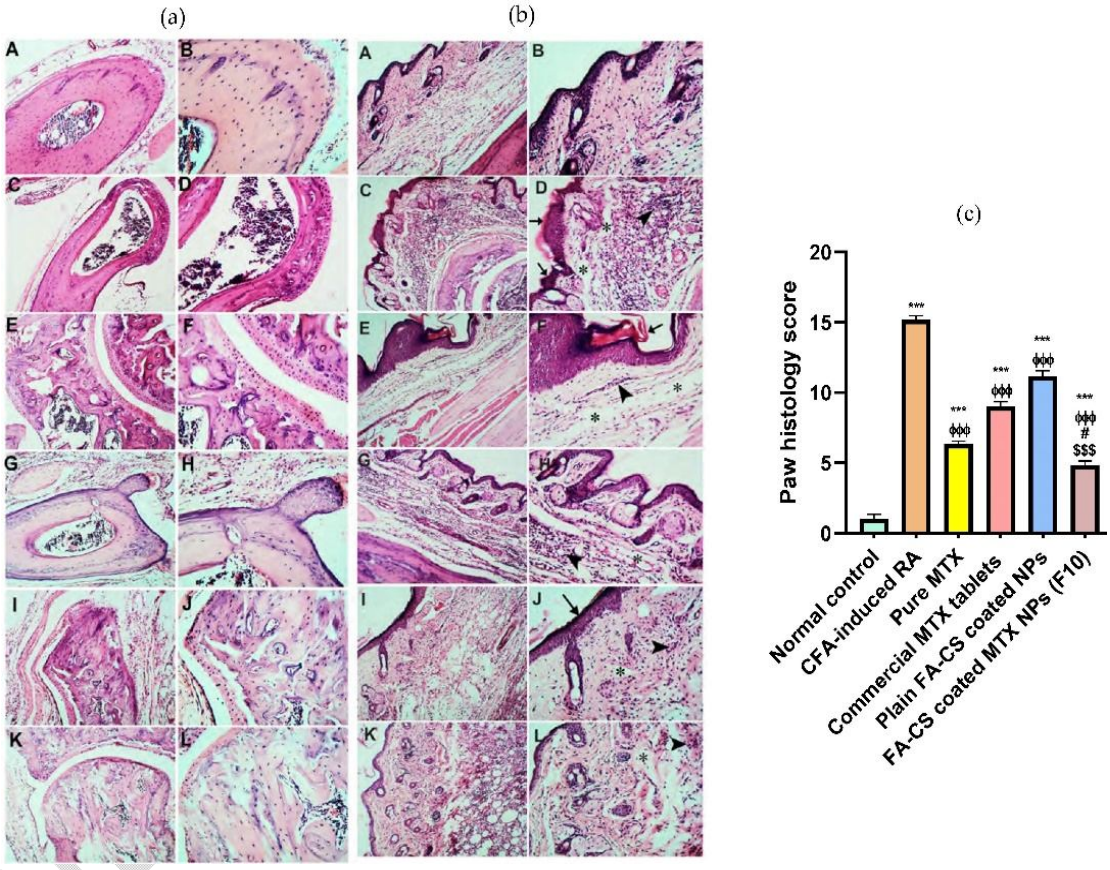

Fig. 9. Representative microphotographs of H&E-stained sections of (a) paw bone, cartilaginous structure and synovial membrane, (b) paw soft tissue, and (c) statistical analysis of the paw histopathology score of H&E-stained section of all experimental groups.

(A & B) Normal control group, (C & D) CFA-induced RA group, (E & F) pure MTX, (G & H) commercial MTX tablets, (I & J) plain FA-CS coated NPs, and (K & L) FA-CS coated MTX NPs (F10) orally treated groups. (A, C, E, G, I & K low magnification X: 200; B, D, F, H, J & L high magnification X: 400). Arrow: hyperkeratosis and epithelial proliferation. Asterix: edema. Arrow head: inflammatory cell infiltration. Data are expressed as the mean ± SEM (n = 6). Statistical significances are indicated as $^{***}p<0.001$ vs normal control group, $^{\phi\phi\phi}p<0.001$ vs CFA-induced RA group, $^{\#}p<0.05$ vs pure MTX treated group, and $^{\$\$\$}p<0.001$ vs commercial MTX tablets treated group.

Such distinguished efficacy noticed from the oral treatment with the optimized FA-CS coated MTX NPs formulation (F10) compared to conventional oral treatment with pure MTX or commercial MTX tablets could be related to various reasons. Firstly, possible increment in oral bioavailability of MTX upon encapsulation in PLGA NPs [16]. Moreover, surface functionalization of MTX PLGA-based nanocarrier with FA-CS conjugate could have synergistically augmented its transcellular transport, intestinal barrier permeation,

and oral bioavailability compared to either pure or commercial MTX tablets. FA could target FR that is found on the surface of intestinal epithelial cells, potentiating the oral absorption of the developed MTX nanocarrier via FR-mediated endocytosis. Recent findings have reported the role of surface functionalization of oral nanocarriers with FA in enhancing the intestinal permeation and the oral absorption and bioavailability of drug payload [64, 84, 85]. Moreover, CS has mucoadhesive and permeability enhancing characteristics, reversibly opening tight junctions between epithelial cells, which could potentially enhance paracellular and transcellular uptake of NPs [15, 35]. Secondly, FA-CS coated MTX NPs formulation (F10) had PS (278.6 nm) that could permit passive targeting of the studied nanocarrier through EPR effect as RA is characterized by highly permeable vasculature and formation of endothelial gaps up to 700 nm [86], resulting in NPs retention and accumulation in inflamed joints. Moreover, the formulated FA-decorated MTX nanocarrier could actively target FR that is upregulated on the surface of activated macrophages accumulating in inflamed joints, augmenting MTX uptake by activated macrophages through receptor mediated endocytosis and enhancing MTX anti-inflammatory effect. Thus, the investigated targeted nanocarrier can allow passive and active targeted delivery of MTX to the desired site of action, which could not be achieved in oral treatment with non-targeted conventional MTX formulations. These findings correlated with previously mentioned results in literature [17, 44]. Additionally, CS has an anti-inflammatory effect, can downregulate the production of pro-inflammatory cytokines, and can stimulate chondrocytes proliferation [83]. Such characters of CS cannot be overlooked and may explain the significant reductions in cytokines levels as well as the noted improvements in the pathological changes seen in the plain FA-CS NPs orally treated group in comparison to those of the untreated mice.

3.6.4 Body Weight Measurments

Serious systemic toxicity can be observed in long term use of MTX, particularly for highly proliferative cells such GI tract and bone marrow [87], resulting in undesirable changes in hematological parameters and body weight loss due to vomiting, diarrhea, nausea, and malabsorption, in addition to nephrotoxicity and hepatotoxicity [19]. Plain FA-CS coated NPs and FA-CS coated MTX coated NPs (F10) orally treated groups showed comparable body weight to that of normal control and CFA-induced RA groups at the end of the study, indicating safety and non-toxicity of the fabricated targeted nanocarrier for drug delivery, Figure 10(A). On the other hand, pure MTX orally treated group displayed significant reduction in the body weight by the end of the experiment compared to normal control ($p<0.001$) and CFA-induced RA group ($p<0.01$). Obviously, MTX encapsulation in the targeted nanocarrier significantly ($p<0.05$) reduced its effect on body weight compared to pure MTX.

3.6.5 Hematological, Biochemical Parameters and Histopathological Investigations

Hematological analysis verified the safety of the constructed targeted nanocarrier by showing no significant effect in any of the studied parameters in plain FA-CS coated NPs orally treated group compared to CFA-induced RA group, Figure 10(B). Obviously, all hematological parameters were significantly ($p<0.001$) decreased in pure MTX orally treated group compared to CFA-induced RA group, indicating MTX associated hematological toxicity, while FA-CS coated MTX NPs (F10) orally treated group showed significant ($p<0.001$) increase in all hematological parameters compared to pure MTX orally treated group. Such results validated the enhanced safety and lowered toxicity of MTX when encapsulated in the fabricated targeted nanocarrier.

Hepatotoxicity and nephrotoxicity associated with oral MTX treatment were assessed by estimating serum levels of ALT, AST, CR, and BUN, Figure 11(a). Pure MTX orally treated group exhibited obvious elevation in serum levels of these biomarkers, which could be attributed to hepatotoxicity and nephrotoxicity associated with MTX treatment. Contrastingly, this elevation was significantly ($p<0.001$) attenuated in FA-CS coated MTX NPs (F10) orally treated group, which exhibited minimal alterations in hepatic and renal markers compared to pure MTX orally treated group.

Microphotographs of H&E stained sections of liver, Figure 11(b), of normal control group showed normal liver tissue architecture with plates of hepatocytes radiating from the central veins. The individual cells show clear acidophilic cytoplasm and vesicular nuclei. In contrast, the CFA-induced RA group showed vacuolation of the cytoplasm of the cells with aggregations of inflammatory cells in the vicinity of the central veins. Pure MTX orally treated group histology was similar to that of CFA-induced RA group with congestion of the central veins. Commercial MTX tablets orally treated group displayed improved hepatic tissue with still vacuolation of the cytoplasm of the hepatocytes with non-congested central veins. Plain FA-CS coated NPs orally treated group showed less pathological alterations than those of the affected groups; however, some hepatocytes still showed vacuolation of the cytoplasm. Oral treatment with FA-CS MTX NPs (F10) showed less pathological damage than that seen in affected groups and did not induce any more tissue damage; it was more or less close to the plain FA-CS NPs treated group, which was consistent with the results of the of hepatic biomarkers.

H&E stained sections of kidney, Figure 11(c), of normal control group showed normal kidney cortices containing the glomeruli, proximal and distal tubules. On the other hand, the CFA-induced RA group showed pale stained glomeruli and vacuolation of the cytoplasm of the endothelial lining of the renal tubules. Renal sections of pure MTX orally treated group depicted focal areas of tubular degeneration and interstitial hemorrhage. Commercial MTX tablets orally treated group showed picture close to that of CFA-induced RA group. However, plain FA-CS coated NPs and FA-CS coated MTX NPs (F10) orally treated groups showed less pathological changes than those in the affected groups; FA-CS coated MTX NPs (F10) orally treated group was more or less close to the normal control group.

Results of biomarkers and histopathological changes of liver and kidney revealed that oral treatment with FA-CS coated MTX NPs formulation (F10) markedly attenuated the toxic effects of MTX, seen in pure MTX group, which indicated the improved safety of MTX when loaded in targeted nanocarrier. This could be attributed to non-selective systemic delivery of pure MTX, while FA-CS coated MTX NPs formulation (F10) was passively, selectively and actively targeted to inflamed joints, thus limiting MTX delivery to

off-target sites, reducing its systemic toxicity. It is worth to mention that commercial MTX tablets orally treated group showed sort of reduced systemic toxicity. Such observation could be related to lower oral bioavailability of MTX from commercial tablets compared to enhanced oral bioavailability of MTX when encapsulated in the investigated targeted nanocarrier; thus, less MTX was available at either target or off-target sites after oral administration of commercial tablets, a suggestion verified by the superior therapeutic performance of the prepared MTX targeted nanocarrier over commercial MTX tablets. Interestingly, plain FA-CS coated NPs orally treated group exhibited a significant (p<0.001) decline in all hepatic and renal biomarkers in addition to improved histopathological features of hepatic and renal sections, Figure 11, compared to those of CFA-induced RA group, which could be attributed to the reported anti-inflammatory and antioxidant effects of CS that could alleviate hepatic abnormalities [35] and could improve renal dysfunction [88]. Foremost, the investigated FA-CS surface decorated MTX nanocarrier portrayed an improvement in therapeutic benefits and a reduction in MTX related systemic toxicity upon oral administration in treatment of CFA-induced RA mice model compared to conventional MTX oral delivery, enhancing MTX therapeutic index. Since drug delivery via oral route is the most favored way for drug administration, the current study presents a promising targeted nanocarrier of MTX for oral treatment of RA that could improve patient overall wellness and enhance patient adherence and compliance motivating further clinical investigations.

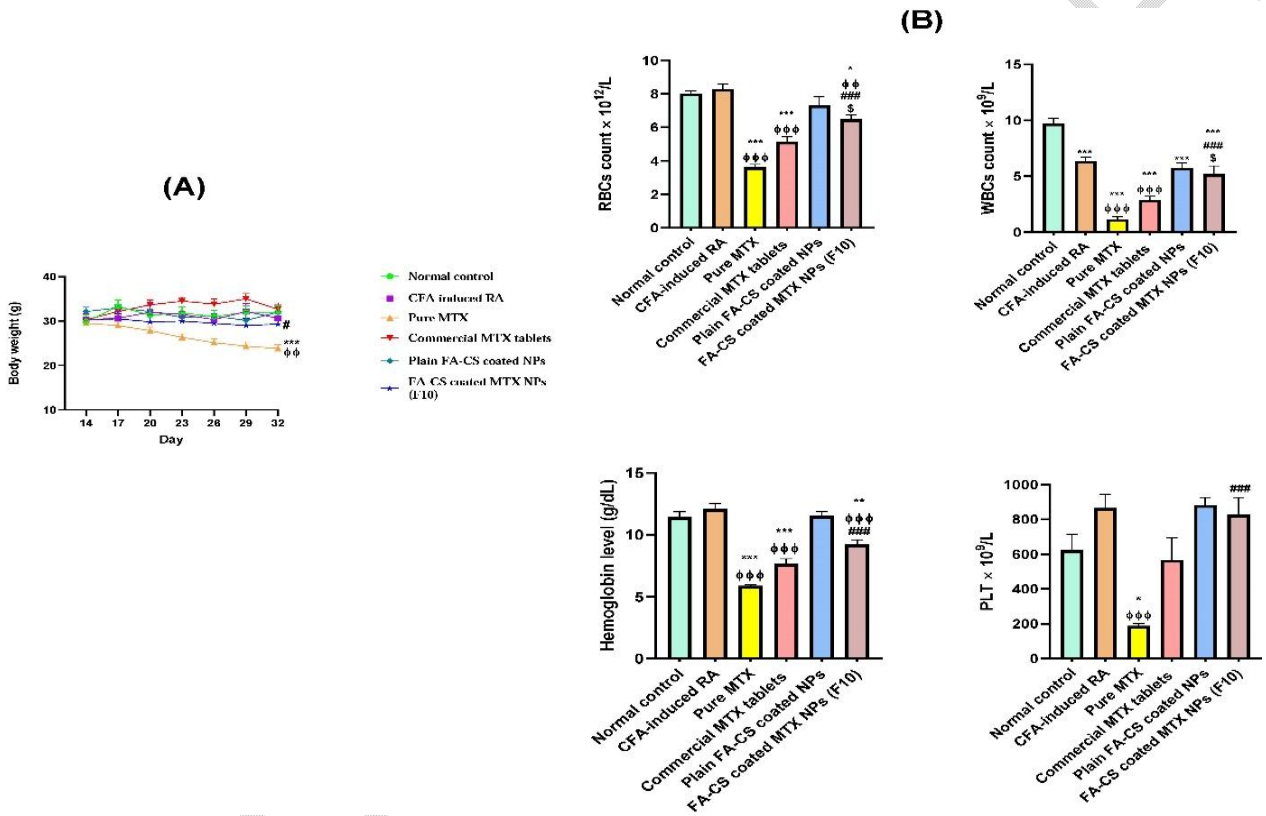

Fig. 10. Safety and systemic toxicity evaluation of the optimized FA-CS coated MTX NPs (F10). (A) Body weight variation of mice in all treated groups since treatment commencement. (B) Evaluation of hematological parameters of mice in all treated groups after different treatments.

Data are expressed as the mean ± SEM (n = 6). Statistical significances are indicated as $^{*}p<0.05$, $^{**}p<0.01$, and $^{***}p<0.001$ vs normal control group, $^{\phi\phi}p<0.01$ and $^{\phi\phi\phi}p<0.001$ vs CFA-induced RA group, $^{\#}p<0.05$ and $^{\#\#\#}p<0.001$ vs pure MTX treated group, $^{\$}p<0.05$ vs commercial MTX tablets treated group.

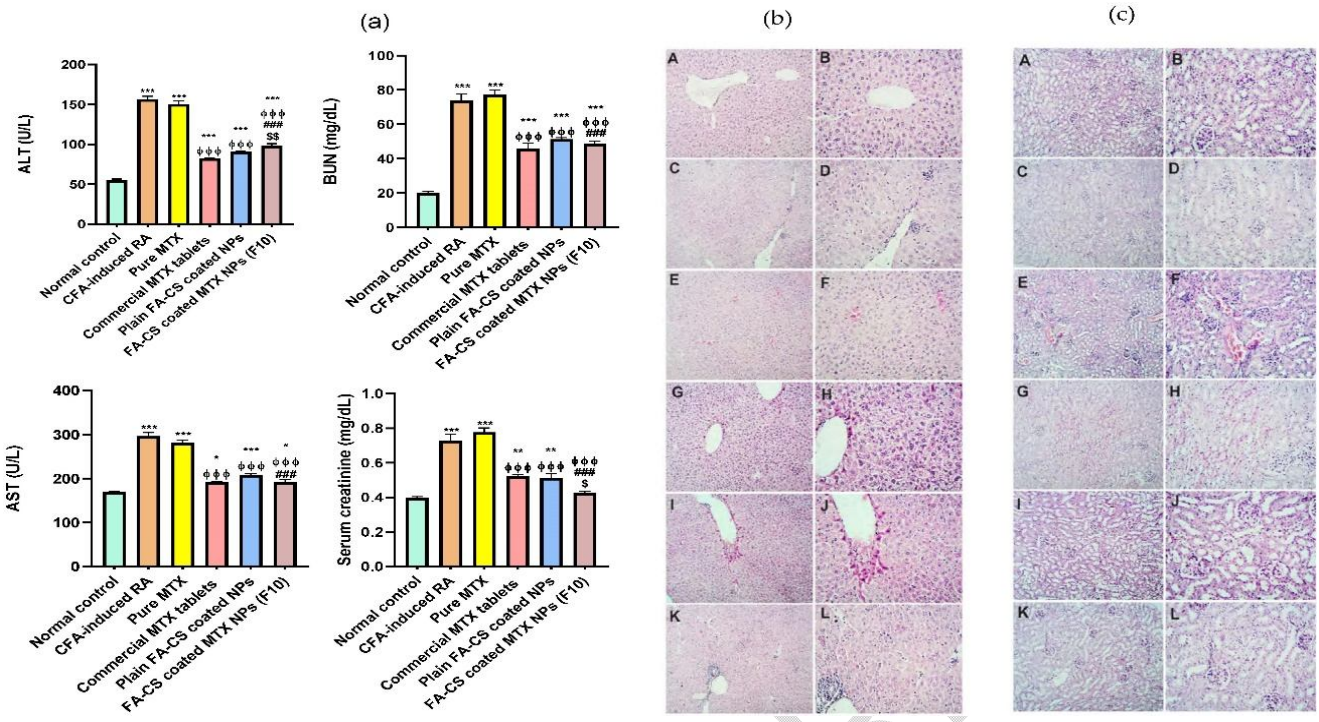

Fig. 11. Assessment of hepatotoxicity and nephrotoxicity of FA-CS coated MTX NPs (F10).

(a) Biochemical parameters of mice after different treatments and (b and c) representative microphotographs of H&E-stained sections of liver and kidney, respectively, of mice after different treatments. (A & B) Normal control group, (C & D) CFA-induced RA group, (E & F) pure MTX, (G & H) commercial MTX tablets, (I & J) plain FA-CS coated NPs, and (K & L) FA-CS coated MTX NPs (F10) orally treated groups. (A, C, E, G, I & K low magnification X: 200; B, D, F, H, J & L high magnification X: 400). Data are expressed as the mean ± SEM (n = 6). Statistical significances are indicated as $^{*}p<0.05$, $^{**}p<0.01$ and $^{***}p<0.001$ vs normal control group, $^{\phi\phi\phi}p<0.001$ vs CFA-induced RA group, $^{\#\#\#}p<0.001$ vs pure MTX treated group, $^{\$}p<0.05$ and $^{\$\$}p<0.01$ vs commercial MTX tablets treated group.

4. CONCLUSION

FA-CS coated PLGA NPs encapsulating cytotoxic drug MTX were auspiciously prepared to target MTX delivery to FR-overexpressing cells. The optimized targeted MTX nanocarrier (F10) had optimum EE% (76.2%), homogenous PS (278.6 nm) and positive ζP (34.0 mV) and showed biphasic drug release in different physiological pHs. FTIR, DSC, and XRD analysis validated MTX encapsulation within the polymeric matrix and the compatability among the formulation components. TEM analysis confirmed spherical structure of the optimized targeted MTX nanocarrier (F10). *In vitro* cytotoxicity assay revealed superior cytotoxicity and lower IC50 values of the prepared targeted MTX nanocarrier than either free MTX or uncoated MTX NPs to FR-positive cancer cells and showed its reduced cytotoxicity to FR-negative cells, confirming the potential of prepared targeted nanocarrier to afford passive and receptor-mediated targeted MTX delivery to FR-overexpressing cancer cells. *In vivo* study in treatment of CFA-induced RA mice model endorsed conspicuous anti-inflammatory efficacy of the fabricated targeted MTX nanocarrier with pronounced reduction in the systemic toxicity of MTX compared to pure MTX and commercial MTX tablets, which portrayed a novel orally administered targeted MTX nanocarrier that could be alternative for conventional oral MTX delivery systems in treatment of RA or other inflammatory conditions associated with activated macrophages. Interestingly, plain targeted nanocarrier formulation exhibited considerable anti-inflammatory effects, proposing promising outcomes in its future application with different drugs in treatment of RA for synergistic benefits. Thus, the targeted nanocarrier adapted in the current investigation can be a novel oral drug delivery system for better therapeutic benefits in management of multitude of autoimmune and inflammatory conditions whose pathogenesis relies on activated macrophages, including psoriasis, atherosclerosis, inflammatory bowl disease.

CONSENT

Not applicable.

ETHICAL APPROVAL

The study was approved by the Research Ethics Committee of Faculty of Pharmacy, Mansoura University, Egypt (Ethical approval code: 2017 - 60). The experiments were conducted in congruity with the National Institute of Health guidelines of "Principles of Laboratory Animal Care" (NIH publication No. 85 - 23, updated 1985).

REFERENCES

1. Bhushan B, Gopinath P. Tumor-targeted folate-decorated albumin-stabilised silver nanoparticles induce apoptosis at low concentration in human breast cancer cells. RSC Advances. 2015;5(105):86242-53.
2. de Moraes Profirio D, Pessine FBT. Formulation of functionalized PLGA nanoparticles with folic acid-conjugated chitosan for carboplatin encapsulation. Eur Polym J. 2018;108:311-21.
3. Fasehee H, Dinarvand R, Ghavamzadeh A, Esfandyari-Manesh M, Moradian H, Faghihi S, et al. Delivery of disulfiram into breast cancer cells using folate-receptor-targeted PLGA-PEG nanoparticles: in vitro and in vivo investigations. J Nanobiotechnology. 2016;14:32.
4. Martín-Sabroso C, Torres-Suarez AI, Alonso-Gonzalez M, Fernandez-Carballido A, Fraguas-Sanchez AI. Active Targeted Nanoformulations via Folate Receptors: State of the Art and Future Perspectives. Pharmaceutics. 2021;14(1):14.
5. Low PS, Henne WA, Doorneweerd DD. Discovery and Development of Folic-Acid-Based Receptor Targeting for Imaging and Therapy of Cancer and Inflammatory Diseases. Acc Chem Res. 2008;41(1):120-9.
6. Kumar V, Leekha A, Kaul A, Mishra AK, Verma AK. Role of folate-conjugated glycol-chitosan nanoparticles in modulating the activated macrophages to ameliorate inflammatory arthritis: in vitro and in vivo activities. Drug Deliv Transl Res. 2020;10(4):1057-75.
7. Li P, Wang Y, Zeng F, Chen L, Peng Z, Kong LX. Synthesis and characterization of folate conjugated chitosan and cellular uptake of its nanoparticles in HT-29 cells. Carbohydr Res. 2011;346(6):801-6.
8. Dhas NL, Ige PP, Kudarha RR. Design, optimization and in-vitro study of folic acid conjugated-chitosan functionalized PLGA nanoparticle for delivery of bicalutamide in prostate cancer. Powder Technol. 2015;283:234-45.
9. Al-Nemrawi NK, Altawabeyeh RM, Darweesh RS. Preparation and Characterization of Docetaxel-PLGA Nanoparticles Coated with Folic Acid-chitosan Conjugate for Cancer Treatment. J Pharm Sci. 2022;111(2):485-94.
10. Vakilinezhad MA, Amini A, Dara T, Alipour S. Methotrexate and Curcumin co-encapsulated PLGA nanoparticles as a potential breast cancer therapeutic system: In vitro and in vivo evaluation. Colloids Surf B Biointerfaces. 2019;184:110515.
11. Alshehri S, Imam SS, Rizwanullah M, Fakhri KU, Rizvi MMA, Mahdi W, et al. Effect of Chitosan Coating on PLGA Nanoparticles for Oral Delivery of Thymoquinone: In Vitro, Ex Vivo, and Cancer Cell Line Assessments. Coatings. 2021;11(1):6.
12. Aman RM, Zaghloul RA, El-Dahhan MS. Formulation, optimization and characterization of allantoin-loaded chitosan nanoparticles to alleviate ethanol-induced gastric ulcer: in-vitro and in-vivo studies. Sci Rep. 2021;11(1):2216.
13. Ji J, Zuo P, Wang YL. Enhanced Antiproliferative Effect of Carboplatin in Cervical Cancer Cells Utilizing Folate-Grafted Polymeric Nanoparticles. Nanoscale Res Lett. 2015;10(1):453.
14. Lu B, Lv X, Le Y. Chitosan-Modified PLGA Nanoparticles for Control-Released Drug Delivery. Polymers (Basel). 2019;11(2):304.
15. Abd El Hady WE, Mohamed EA, Soliman OAE, El-Sabbagh HM. In vitro-in vivo evaluation of chitosan-PLGA nanoparticles for potentiated gastric retention and anti-ulcer activity of diosmin. Int J Nanomedicine. 2019;14:7191-213.
16. Jang JH, Jeong SH, Lee YB. Preparation and In Vitro/In Vivo Characterization of Polymeric Nanoparticles Containing Methotrexate to Improve Lymphatic Delivery. Int J Mol Sci. 2019;20(13):3312.
17. Li X, Wang H, Zou X, Su H, Li C. Methotrexate-loaded folic acid of solid-phase synthesis conjugated gold nanoparticles targeted treatment for rheumatoid arthritis. Eur J Pharm Sci. 2022;170:106101.
18. Chen H, Sun Y, Xu X, Ye Q. Targeted delivery of methotrexate by modified yeast beta-glucan nanoparticles for rheumatoid arthritis therapy. Carbohydr Polym. 2022;284:119183.
19. Wang X, Cao W, Sun C, Wang Y, Wang M, Wu J. Development of pH-sensitive dextran-based methotrexate nanodrug for rheumatoid arthritis therapy through inhibition of JAK-STAT pathways. Int J Pharm. 2022;622:121874.
20. Issarachot O, Suksiriworapong J, Takano M, Yumoto R, Junyaprasert VB. Folic acid-modified methotrexate-conjugated PEGylated poly(ε-caprolactone) nanoparticles for targeted delivery. J Nanopart Res. 2014;16(2):2276.

21. Hashad RA, Ishak RA, Geneidi AS, Mansour S. Surface functionalization of methotrexate-loaded chitosan nanoparticles with hyaluronic acid/human serum albumin: Comparative characterization and in vitro cytotoxicity. Int J Pharm. 2017;522(1-2):128-36.
22. Nguyen HT, Phung CD, Thapa RK, Pham TT, Tran TH, Jeong J-H, et al. Multifunctional nanoparticles as somatostatin receptor-targeting delivery system of polyaniline and methotrexate for combined chemo–photothermal therapy. Acta Biomater. 2018;68:154-67.
23. Pandey S, Rai N, Mahtab A, Mittal D, Ahmad FJ, Sandal N, et al. Hyaluronate-functionalized hydroxyapatite nanoparticles laden with methotrexate and teriflunomide for the treatment of rheumatoid arthritis. Int J Biol Macromol. 2021;171:502-13.
24. Panonnummal R, Jayakumar R, Anjaneyan G, Sabitha M. In vivo anti-psoriatic activity, biodistribution, sub-acute and sub-chronic toxicity studies of orally administered methotrexate loaded chitin nanogel in comparison with methotrexate tablet. Int J Biol Macromol. 2018;110:259-68.
25. Ji J, Wu D, Liu L, Chen J, Xu Y. Preparation, characterization, and in vitro release of folic acid-conjugated chitosan nanoparticles loaded with methotrexate for targeted delivery. Polym Bull. 2011;68(6):1707-20.
26. Massadeh S, Alaamery M, Al-Qatanani S, Alarifi S, Bawazeer S, Alyafee Y. Synthesis of protein-coated biocompatible methotrexate-loaded PLA-PEG-PLA nanoparticles for breast cancer treatment. Nano Rev Exp. 2016;7(1):31996.
27. Vakilinezhad MA, Alipour S, Montaseri H. Fabrication and in vitro evaluation of magnetic PLGA nanoparticles as a potential Methotrexate delivery system for breast cancer. J Drug Deliv Sci Technol. 2018;44:467-74.
28. Al-Nemrawi N, Hameedat F, Al-Husein B, Nimrawi S. Photolytic Controlled Release Formulation of Methotrexate Loaded in Chitosan/TiO(2) Nanoparticles for Breast Cancer. Pharmaceuticals (Basel). 2022;15(2).
29. Esim O, Oztuna A, Sarper M, Hascicek C. Chitosan-coated bovine serum albumin nanocarriers mediate efficient delivery of methotrexate in breast cancer therapeutics. J Drug Deliv Sci Technol. 2022;77:103906.
30. Higuchi T. Mechanism of sustained-action medication. Theoretical analysis of rate of release of solid drugs dispersed in solid matrices. J Pharm Sci. 1963;52:1145-9.
31. Ritger PL, Peppas NA. A simple equation for description of solute release I. Fickian and non-fickian release from non-swellable devices in the form of slabs, spheres, cylinders or discs. J Control Release. 1987;5(1):23-36.
32. Martin AN, Bustamante P, Chun AHC. Physical Pharmacy: Physical Chemical Principles in the Pharmaceutical Sciences. 4th ed. Philadelphia: Lea & Febiger; 1993.
33. Oransa HA, Boughdady MF, El-Sabbagh HM. Novel Mucoadhesive Chitosomes as a Platform for Enhanced Oral Bioavailability of Cinnarizine. Int J Nanomedicine. 2022;17:5641-60.
34. Awadeen RH, Boughdady MF, Meshali MM. Quality by Design Approach for Preparation of Zolmitriptan/Chitosan Nanostructured Lipid Carrier Particles - Formulation and Pharmacodynamic Assessment. Int J Nanomedicine. 2020;15:8553-68.
35. Mohamed Anter H, Mokhtar Aman R, Abdelaziz Shaaban A, Ibrahim Abu Hashim I, Mohamed Meshali M. Propitious maneuvering for delivery of the phytopharmaceutical "apocynin" to induced fulminant hepatitis in BALB/c mice: In vitro and in vivo assessments. Int J Pharm. 2022;626:122165.
36. El-Tanbouly GS, Abdelrahman RS. Novel anti-arthritic mechanisms of trans-cinnamaldehyde against complete Freund's adjuvant-induced arthritis in mice: involvement of NF-small ka, CyrillicB/TNF-alpha and IL-6/IL-23/ IL-17 pathways in the immuno-inflammatory responses. Inflammopharmacology. 2022;30(5):1769-80.
37. Nornberg AB, Martins CC, Cervi VF, Sari MHM, Cruz L, Luchese C, et al. Transdermal release of methotrexate by cationic starch/poly(vinyl alcohol)-based films as an approach for rheumatoid arthritis treatment. Int J Pharm. 2022;611:121285.
38. Saad KM, Shaker ME, Shaaban AA, Abdelrahman RS, Said E. The c-Met inhibitor capmatinib alleviates acetaminophen-induced hepatotoxicity. Int Immunopharmacol. 2020;81:106292.
39. Zhong S, Liu P, Ding J, Zhou W. Hyaluronic Acid-Coated MTX-PEI Nanoparticles for Targeted Rheumatoid Arthritis Therapy. Crystals. 2021;11(4):321.
40. Silva MD, Savinainen A, Kapadia R, Ruan J, Siebert E, Avitahl N, et al. Quantitative Analysis of Micro-CT Imaging and Histopathological Signatures of Experimental Arthritis in Rats. Mol Imaging. 2004;3(4):312-318.

41. Othman SH, Ibrahim IA, Hatab MH, Elbarbary AM. Preparation, characterization and biodistribution in quails of (99m)Tc-folic acid/chitosan nanostructure. Int J Biol Macromol. 2016;92:550-60.
42. Singh RP, Sharma G, Sonali, Singh S, Bharti S, Pandey BL, et al. Chitosan-folate decorated carbon nanotubes for site specific lung cancer delivery. Mater Sci Eng C Mater Biol Appl. 2017;77:446-58.
43. Radnia F, Mohajeri N, Hashemi F, Imani M, Zarghami N. Design and development of folate-chitosan/CD nanogel: An efficient fluorescent platform for Cancer-specific delivery of AntimiR-21. React Funct Polym. 2021;160:104814.
44. Zewail M. Folic acid decorated chitosan-coated solid lipid nanoparticles for the oral treatment of rheumatoid arthritis. Ther Deliv. 2021;12(4):297-310.
45. Amiryaghoubi N, Abdolahinia ED, Nakhlband A, Aslzad S, Fathi M, Barar J, et al. Smart chitosan-folate hybrid magnetic nanoparticles for targeted delivery of doxorubicin to osteosarcoma cells. Colloids Surf B Biointerfaces. 2022;220:112911.
46. Geethakumari D, Bhaskaran Sathyabhama A, Raji Sathyan K, Mohandas D, Somasekharan JV, Thavarool Puthiyedathu S. Folate functionalized chitosan nanoparticles as targeted delivery systems for improved anticancer efficiency of cytarabine in MCF-7 human breast cancer cell lines. Int J Biol Macromol. 2022;199:150-61.
47. El-Leithy ES, Abdel-Bar HM, el-Moneum RA. Synthesis, Optimization and Characterization of Folate-Chitosan polymer conjugate for Possible Oral delivery of Macromolecular drugs. IOSR J Pharm. 2017; 7(1):30-8.
48. Anter HM, Aman RM, Othman DIA, Elamin KM, Hashim IIA, Meshali MM. Apocynin-loaded PLGA nanomedicine tailored with galactosylated chitosan intrigue asialoglycoprotein receptor in hepatic carcinoma: Prospective targeted therapy. Int J Pharm. 2023;631:122536.
49. Batinić PM, Đorđević VB, Stevanović SI, Balanč BD, Marković SB, Luković ND, et al. Formulation and characterization of novel liposomes containing histidine for encapsulation of a poorly soluble vitamin. J Drug Deliv Sci Technol. 2020;59:101920.
50. Elsewedy HS, Dhubiab BEA, Mahdy MA, Elnahas HM. Development, optimization, and evaluation of PEGylated brucine-loaded PLGA nanoparticles. Drug Deliv. 2020;27(1):1134-46.
51. Karimi Z, Taymouri S, Minaiyan M, Mirian M. Evaluation of thermosensitive chitosan hydrogel containing gefitinib loaded cellulose acetate butyrate nanoparticles in a subcutaneous breast cancer model. Int J Pharm. 2022;624:122036.
52. Duranoğlu D, Uzunoglu D, Mansuroglu B, Arasoglu T, Derman S. Synthesis of hesperetin-loaded PLGA nanoparticles by two different experimental design methods and biological evaluation of optimized nanoparticles. Nanotechnology. 2018;29(39):395603.
53. Sathyamoorthy N, Magharla D, Chintamaneni P, Vankayalu S. Optimization of paclitaxel loaded poly (ε-caprolactone) nanoparticles using Box Behnken design. Beni-Suef univ j basic appl sci. 2017;6(4):362-73.
54. Wang F, Wang Y, Ma Q, Cao Y, Yu B. Development and characterization of folic acid-conjugated chitosan nanoparticles for targeted and controlled delivery of gemcitabinein lung cancer therapeutics. Artif Cells Nanomed Biotechnol. 2017;45(8):1530-8.
55. Haider M, Elsherbeny A, Jagal J, Hubatova-Vackova A, Saad Ahmed I. Optimization and Evaluation of Poly(lactide-co-glycolide) Nanoparticles for Enhanced Cellular Uptake and Efficacy of Paclitaxel in the Treatment of Head and Neck Cancer. Pharmaceutics. 2020;12(9):828.
56. Chourasiya V, Bohrey S, Pandey A. Formulation, optimization, and characterization of amlodipine besylate loaded polymeric nanoparticles. Polym Polym Compos. 2021;29(9_suppl):S1555-S68.
57. Haider T, Soni V. “Response surface methodology and artificial neural network-based modeling and optimization of phosphatidylserine targeted nanocarriers for effective treatment of cancer: In vitro and in silico studies”. J Drug Deliv Sci Technol. 2022;75:103663.
58. Sharma D, Sharma RK, Sharma N, Gabrani R, Sharma SK, Ali J, et al. Nose-To-Brain Delivery of PLGA-Diazepam Nanoparticles. AAPS PharmSciTech. 2015;16(5):1108-21.
59. Radwan SE, El-Kamel A, Zaki EI, Burgalassi S, Zucchetti E, El-Moslemany RM. Hyaluronic-Coated Albumin Nanoparticles for the Non-Invasive Delivery of Apatinib in Diabetic Retinopathy. Int J Nanomedicine. 2021;16:4481-94.
60. Ramalho MJ, Loureiro JA, Coelho MAN, Pereira MC. Factorial Design as a Tool for the Optimization of PLGA Nanoparticles for the Co-Delivery of Temozolomide and O6-Benzylguanine. Pharmaceutics. 2019;11(8):401.

61. Al-Nemrawi NK, Alshraiedeh NH, Zayed AL, Altaani BM. Low Molecular Weight Chitosan-Coated PLGA Nanoparticles for Pulmonary Delivery of Tobramycin for Cystic Fibrosis. Pharmaceuticals (Basel). 2018;11(1):28.
62. Mitchell MJ, Billingsley MM, Haley RM, Wechsler ME, Peppas NA, Langer R. Engineering precision nanoparticles for drug delivery. Nat Rev Drug Discov. 2021;20(2):101-24.
63. Motawea A, Ahmed DAM, El-Mansy AA, Saleh NM. Crucial Role of PLGA Nanoparticles in Mitigating the Amiodarone-Induced Pulmonary Toxicity. Int J Nanomedicine. 2021;16:4713-37.
64. Granja A, Vieira AC, Chaves LL, Nunes C, Neves AR, Pinheiro M, et al. Folate-targeted nanostructured lipid carriers for enhanced oral delivery of epigallocatechin-3-gallate. Food Chem. 2017;237:803-10.
65. Gebreel RM, Edris NA, Elmofty HM, Tadros MI, El-Nabarawi MA, Hassan DH. Development and Characterization of PLGA Nanoparticle-Laden Hydrogels for Sustained Ocular Delivery of Norfloxacin in the Treatment of Pseudomonas Keratitis: An Experimental Study. Drug Des Devel Ther. 2021;15:399-418.
66. Teaima MH, Helal DA, Alsofany JM, El-Nabarawi MA, Yasser M. Ion-Triggered In Situ Gelling Intranasal Spray of Dronedarone Hydrochloride Nanocarriers: In Vitro Optimization and In Vivo Pharmacokinetic Appraisal. Pharmaceutics. 2022;14(11):2405.
67. Murugan K, Choonara YE, Kumar P, Bijukumar D, du Toit LC, Pillay V. Parameters and characteristics governing cellular internalization and trans-barrier trafficking of nanostructures. Int J Nanomedicine. 2015;10:2191-206.
68. Nogueira DR, Tavano L, Mitjans M, Perez L, Infante MR, Vinardell MP. In vitro antitumor activity of methotrexate via pH-sensitive chitosan nanoparticles. Biomaterials. 2013;34(11):2758-72.
69. Yu W-J, Huang D-X, Liu S, Sha Y-L, Gao F-h, Liu H. Polymeric Nanoscale Drug Carriers Mediate the Delivery of Methotrexate for Developing Therapeutic Interventions Against Cancer and Rheumatoid Arthritis. Front Oncol. 2020;10:1734.
70. Jang JH, Jeong SH, Lee YB. Enhanced Lymphatic Delivery of Methotrexate Using W/O/W Nanoemulsion: In Vitro Characterization and Pharmacokinetic Study. Pharmaceutics. 2020;12(10):978.
71. Cheng L, Ma H, Shao M, Fan Q, Lv H, Peng J, et al. Synthesis of folate□chitosan nanoparticles loaded with ligustrazine to target folate receptor positive cancer cells. Mol Med Rep. 2017;16(2):1101-8.
72. Hashad RA, Ishak RAH, Geneidi AS, Mansour S. Methotrexate loading in chitosan nanoparticles at a novel pH: Response surface modeling, optimization and characterization. Int J Biol Macromol. 2016;91:630-9.
73. Arafa MG, Mousa HA, Afifi NN. Preparation of PLGA-chitosan based nanocarriers for enhancing antibacterial effect of ciprofloxacin in root canal infection. Drug Deliv. 2020;27(1):26-39.
74. Waly AL, Abdelghany AM, Tarabiah AE. Study the structure of selenium modified polyethylene oxide/polyvinyl alcohol (PEO/PVA) polymer blend. J Mater Res Technol. 2021;14:2962-9.
75. Saleh N, Elshaer S, Girgis G. Biodegradable Polymers-based Nanoparticles to Enhance the Antifungal Efficacy of Fluconazole against Candida albicans. Curr Pharm Biotechnol. 2022;23(5):749-57.
76. Elsayed SI, Girgis GNS, El-Dahan MS. Formulation and Evaluation of Pravastatin Sodium-Loaded PLGA Nanoparticles: In vitro-in vivo Studies Assessment. Int J Nanomedicine. 2023;18:721-42.
77. Garg NK, Tyagi RK, Singh B, Sharma G, Nirbhavane P, Kushwah V, et al. Nanostructured lipid carrier mediates effective delivery of methotrexate to induce apoptosis of rheumatoid arthritis via NF-kappaB and FOXO1. Int J Pharm. 2016;499(1-2):301-20.
78. Seju U, Kumar A, Sawant KK. Development and evaluation of olanzapine-loaded PLGA nanoparticles for nose-to-brain delivery: In vitro and in vivo studies. Acta Biomater. 2011;7(12):4169-76.
79. Joseph C, Daniels A, Singh S, Singh M. Histidine-Tagged Folate-Targeted Gold Nanoparticles for Enhanced Transgene Expression in Breast Cancer Cells In Vitro. Pharmaceutics. 2021;14(1):53.
80. Yücel O, Sengelen A, Emik S, Onay-Ucar E, Arda N, Gurdag G. Folic acid-modified methotrexate-conjugated gold nanoparticles as nano-sized trojans for drug delivery to folate receptor-positive cancer cells. Nanotechnology. 2020;31(35):355101.
81. Soe ZC, Poudel BK, Nguyen HT, Thapa RK, Ou W, Gautam M, et al. Folate-targeted nanostructured chitosan/chondroitin sulfate complex carriers for enhanced delivery of bortezomib to colorectal cancer cells. Asian J Pharm Sci. 2019;14(1):40-51.
82. Xu Q, Zhou Y, Zhang R, Sun Z, Cheng LF. Antiarthritic Activity of Qi-Wu Rheumatism Granule (a Chinese Herbal Compound) on Complete Freund's Adjuvant-Induced Arthritis in Rats. Evid Based Complement Alternat Med. 2017;2017:1960517.
83. Zewail M, Nafee N, Helmy MW, Boraie N. Coated nanostructured lipid carriers targeting the joints – An effective and safe approach for the oral management of rheumatoid arthritis. Int J Pharm. 2019;567:118447.

84. Jain S, Rathi VV, Jain AK, Das M, Godugu C. Folate-decorated PLGA nanoparticles as a rationally designed vehicle for the oral delivery of insulin. Nanomedicine (Lond). 2012;7(9):1311-37.
85. Granja A, Neves AR, Sousa CT, Pinheiro M, Reis S. EGCG intestinal absorption and oral bioavailability enhancement using folic acid-functionalized nanostructured lipid carriers. Heliyon. 2019;5(7):e02020.
86. Yang M, Feng X, Ding J, Chang F, Chen X. Nanotherapeutics relieve rheumatoid arthritis. J Control Release. 2017;252:108-24.
87. Qi R, Majoros I, Misra AC, Koch AE, Campbell P, Marotte H, et al. Folate Receptor-Targeted Dendrimer-Methotrexate Conjugate for Inflammatory Arthritis. J Biomed Nanotechnol. 2015;11(8):1431-41.
88. Nomier YA, Alshahrani S, Elsabahy M, Asaad GF, Hassan A, El-Dakroury WA. Ameliorative effect of chitosan nanoparticles against carbon tetrachloride-induced nephrotoxicity in Wistar rats. Pharm Biol. 2022;60(1):2134-44.